

AD-A274 029



①

AFIT/GE/ENG/93D-09

DTIC
ELECTE
DEC 23 1993
S A

**ANALYZING ADAPTIVE BEAMFORMER PERFORMANCE
IN A STABLE MULTIPATH ENVIRONMENT**

THESIS
Mark Godino
Captain, USAF

AFIT/GE/ENG/93D-09

Approved for public release; distribution unlimited

93 12 22 131

93-31018

The views expressed in this thesis are those of the author and do not reflect the official policy or position of the Department of Defense or the U. S. Government.

Accession For	
NTIS CRA&I	<input checked="checked" type="checkbox"/>
DTIC TAB	<input type="checkbox"/>
Unannounced	<input type="checkbox"/>
Justification	
By	
Distribution /	
Availability Codes	
Dist	Avail and/or Special
A-1	

DTIC QUALITY INSPECTED 3

AFIT/GE/ENG/93D-09

**ANALYZING ADAPTIVE BEAMFORMER PERFORMANCE
IN A STABLE MULTIPATH ENVIRONMENT**

THESIS

**Presented to the Faculty of the Graduate School of Engineering
of the Air Force Institute of Technology
Air University
In Partial Fulfillment of the
Requirements for the Degree of
Master of Science in Electrical Engineering**

**Mark Godino, B.E., B.S.E.E, M.S.M.SC.
Captain, USAF**

December, 1993

Approved for public release; distribution unlimited

Acknowledgements

This work was sponsored by Wright Laboratory, WL/AARM-3 at Wright-Patterson AFB. I thank Richard A. Kitzerow from the above organization for inviting me to contractor presentations on the study topic and providing background material necessary to complete this task. I would like to thank my advisor, Dr. Michael P. Clark for the help in learning the underlying mathematics, notation, and fundamental signal processing/beamforming concepts, which allowed me to study the problem and complete this thesis. Also, I'd like to acknowledge Captain Joseph Sacchini and Captain Ronald DeLap, the other members of my thesis committee who reviewed this work. I thank the members of the GE-93D Communications/Radar track, for their help in teaching me how to use LaTeX. I especially thank Captain Lynn C. King for allowing me to use his Latex templates for the thesis document and presentation slides; these helped me to quickly document my work and finish on time. Lastly, I wish to thank my wife, Lynn, who stood by me and supported me.

Mark Godino

Table of Contents

	Page
Acknowledgements	ii
List of Figures	v
Abstract	vi
 I. Introduction	 1-1
1.1 Background	1-1
1.2 Problem	1-1
1.3 Assumptions	1-2
1.4 Scope	1-2
1.5 Approach	1-2
 II. Literature Review	 2-1
 III. Preliminaries	 3-1
3.1 Introduction	3-1
3.2 Basic Definitions	3-1
3.3 Basic Concepts	3-2
3.3.1 Narrowband Beamforming	3-2
3.3.2 Broadband Beamforming	3-8
3.4 Data Generation	3-12
3.5 Linear Constraint Design	3-13
3.6 Linearly Constrained Minimum Variance (LCMV) Beamforming . . .	3-14
3.6.1 LCMV Criterion	3-14
3.6.2 Generalized Sidelobe Canceller	3-15

	Page
IV. Analysis and Simulations	4-1
4.1 Introduction	4-1
4.2 Narrowband Beamforming	4-1
4.2.1 Data Generation	4-1
4.2.2 Point Constraints	4-7
4.3 Broadband Beamforming	4-10
4.3.1 Data Generation	4-10
4.3.2 Eigenvector Constraints	4-22
V. Conclusions and Recommendations	5-1
Appendix A. MATLAB Code	A-1
Bibliography	BIB-1
Vita	VITA-1

List of Figures

Figure	Page
3.1. Narrowband beamformer	3-2
3.2. Broadband beamformer	3-8
3.3. Generalized sidelobe canceller schematic	3-15
4.1. Two plate multipath model	4-5
4.2. Narrowband beamformer with eight interferers; SNR = INR = 60 dB	4-7
4.3. Narrowband beampattern for multipath case	4-8
4.4. Output power with quiescent weights; SNR = 60 dB	4-9
4.5. Output power with adapted weights	4-9
4.6. Two plate multipath model	4-16
4.7. Gain of beamformer with correlated signals as a function of DOA for constraint over frequency interval $[2\pi/5, 4\pi/5]$ at -45 degrees plotted at nine frequencies .	4-29
4.8. Beampattern displaying reflection lobe; SNR = 20 dB	4-31
4.9. Normalized output power with quiescent weights	4-31
4.10. Normalized output power with adapted weights	4-32
4.11. Cancellation as a function of the ratio of temporal aperture ($T(\theta)$) to path delay ($del(\theta)$)	4-33

Abstract

The enemy's synergistic deployment of low observable (LO) airborne threats and stand-off/escort jammers may defeat USAF fighter/interceptor air-to-air radars. A potential solution to this problem is to employ an adaptive beamformer. An adaptive beamformer can be used to cancel interferences while allowing desired signals to be passed from other directions. The jamming signal can be eliminated by either 1) placing a null in the direction of the jammer, or 2) coherently cancelling the jamming signal.

Fighter aircraft equipped with X-Band radars having an adaptive beamforming capability exhibit degraded performance due to radome multipath reflections (RMR). The reflections from the radome into the antenna array degrade the pattern by causing the formation of large sidelobes. This phenomenon makes detection of LO targets difficult when jamming enters the high RMR sidelobes. The combination of broadband jammers and the radar operating in a high-resolution mode (wide frequency bandwidth) requires a broadband beamformer to solve the problem. Future low radar cross section (RCS) radomes will degrade the beampattern even more, making the problem worse. Actual radomes are curved and cause reflected wavefronts to be nonplanar. Analyzing beamformer performance under these conditions is difficult, since the beamformer response is defined as the amplitude and phase change experienced by a complex plane wave as a function of frequency and location. To work with planar wavefronts and for the sake of simplicity, we model the radome as two flat plates parallel to array broadside (one at each end of the array). This radome model demonstrates degraded beamformer performance by causing large sidelobes to form. This approximates the characteristics of the multipath environment caused by a real radome. The ability of a linearly constrained, minimum variance beamformer to cancel interference arriving in the sidelobes is evaluated. The cancellation performance depends on how many taps are employed and the source frequency bandwidth.

ANALYZING ADAPTIVE BEAMFORMER PERFORMANCE IN A STABLE MULTIPATH ENVIRONMENT

I. Introduction

1.1 Background

The enemy's synergistic deployment of low observable (LO) airborne threats and stand-off/escort jammers may defeat USAF fighter/interceptor air-to-air radars. A potential solution to this problem is to employ an adaptive beamformer, which consists of an antenna array with weights. An adaptive beamformer can be used to cancel interferences while passing desired signals from other directions. The jamming signal can be eliminated by either 1) placing a null in the direction of the jammer, or 2) coherently cancelling the jamming signal.

1.2 Problem

The presence of the aircraft radome in front of radar antennas degrades adaptive beamformer performance. The reflections from the radome into the antenna array degrade the pattern by causing the formation of large sidelobes. This phenomenon makes detection of LO targets difficult when jamming enters the high RMR lobes. These RMR sidelobes form because energy reflects into the main and other high gain beams. If a jammer is located in the direction of a high RMR sidelobe, a large amount of the beamformer output power will be due to energy reflected into the main beam. In this case a null formed in the direction of the jammer will not attenuate interferer energy which enters the main beam. One solution is to put a null in the main beam. This is not a good idea because this causes desired signals to also be attenuated. Thus, jammer signals must be coherently cancelled so that desired signals can be detected.

1.3 Assumptions

All data are assumed to be wide sense stationary (WSS), which means the data covariance matrix is independent of time. The data received by the array are assumed to be zero mean. All desired signals are assumed to be uncorrelated with all interfering signals. The signals and interferers are uncorrelated with the noise, which is white. The sources are assumed to originate as points in the far field.

The radome is assumed to be perfectly smooth; no random phase is associated with reflecting off the plates. The signal is only attenuated in amplitude. Only a single bounce off the plate into the array is analyzed. All discussion of frequency is in terms of normalized frequency.

1.4 Scope

The scope of this thesis is limited to modeling the radome as two flat plates. The direct path signal through the first plate and the first bounce signal off the second plate are generated and used as input to a fully adaptive beamformer. The output power as a function of the number of taps is calculated to determine the amount of interference cancellation obtained.

1.5 Approach

The radome is modeled to simulate its effect on beamformer performance. Since beamformer response is defined in terms of the amplitude and phase change experienced by a complex plane wave as a function of frequency and location, a radome model which supports plane waves is developed. The radome is modeled as two flat plates with reflection coefficients which are functions of angle. This radome model is used to simulate the RMR environment.

The beamformer to be analyzed consists of an equally spaced, linear array of antenna elements along with weights. The number of antenna elements and taps (in the broadband case) is variable. Taps are added behind each sensor in the broadband case to provide for frequency

domain filtering over the signal bandwidth. For a detailed discussion on nonzero bandwidth signals and analysis of tapped delay-line arrays, see Compton's book [9]. The criteria for weight selection is linearly constrained, power minimization, also referred to as linearly constrained, minimum variance (LCMV) beamforming. Before evaluating beamformers in a multipath environment, narrowband and broadband beamformers are designed and validated by comparing results to those in the literature.

Using the radome model described above, a RMR environment is generated . A jammer is placed in a large RMR sidelobe, so that energy reflects into the main beam. The ability of the beamformer to cancel this jamming signal is evaluated by observing the output power of the beamformer in the direction of the jammer.

II. Literature Review

This section presents a summary of research in the area of adaptive beamforming. It starts out with general beamforming concepts and then reviews data generation and other more specific topics related to the subject of this thesis.

Van Veen and Buckley wrote an article on the general concepts involved in beamforming [45]. This article presents the concepts on linearly constrained minimum variance (LCMV) beamforming used in this thesis. In particular, we use the generalized sidelobe canceller (GSC) form of the LCMV beamformer. The GSC is the most general form of adaptive beamformer and has demonstrated better results than any of the specific beamformers such as the multiple sidelobe canceller (MSC) [46]. The MSC can be represented as a specific example of a GSC. The LCMV beamformer approach is preferred since it doesn't assume a partially adaptive solution like the MSC does. By starting with the more general GSC, a partially adaptive solution based on the expected interference environment can be determined. Van Veen and Buckley [45] cover adaptive algorithms and implementation issues which are not discussed as part of this thesis. Van Veen also wrote a chapter in a book on minimum variance beamforming [40]. This material is updated from his previous articles. It presents some new information which makes the derivations easier to follow.

Most of the research in the area of beamforming assumes narrowband signals and doesn't discuss the details of broadband beamforming. Buckley wrote an article on broadband beamforming which develops models for broadband sources [5]. This article, along with those of Van Veen, provides all the details necessary to design narrowband and broadband beamformers. It also describes models for uncorrelated broadband signals with spatial and/or frequency extent.

Compton's article and book provide an explanation of broadband interference cancellation performance using tapped delay lines [8][9]. Monzingo and Miller also discuss broadband concepts [30]. They discuss practical aspects of adaptive arrays and include many of the mathematical derivations.

Dudgeon's article covers the fundamentals of digital array processing [10]; it applies basic digital signal processing principles to beamforming. His book [11] contains multidimensional signal processing ideas applied to beamforming. It describes the delay-and-sum beamformer, which is used in this thesis. The section on wavenumber-frequency space filtering was applied to take advantage of the fast Fourier transform (FFT) in computing the beamformer response. Another book, by Widrow and Stearns [51], covers the fundamentals of adaptive signal processing. It covers basic adaptive systems and their applications, including beamforming. Alexander's book [1] covers adaptive signal processing in more detail than Widrow and Stearns, but doesn't include beamforming applications.

Haykin wrote a chapter in a book [24] on narrowband signal and noise models for radar array processing applications. He describes how off-diagonal elements in the spatial correlation matrix of the signal-in-space vector are all zero and the spatial correlation matrix of the received signal vector is a Toeplitz matrix when the sources are jointly uncorrelated or noncoherent. The spatial correlation matrix of the received signal vector is non-Toeplitz when the sources are correlated or coherent. One method of decorrelating a desired signal from an interferer is based on restoring the Toeplitz structure of the received signal vector [17]. He describes a narrowband multipath model in detail. Haykin also edited a book [18] which contains several articles on array processing applications to radar. Nitzberg's recently published book [32] covers array signal processing for radar. It emphasizes multiple sidelobe cancellers, but discusses topics of equal concern to linearly constrained beamformers. A book by Hudson [22] has several sections dealing with coherent signals, including multipath, and their effects on cancellation performance. It contains discussions not found in the other sources. It also contains some relevant and useful vector, matrix, and statistics properties in the appendices.

Scharf's book [35] contains compact, narrowband models for linear combinations of vectors, including one for the data matrix associated with multisensor arrays. The sections on unitary decomposition, singular value decomposition, and low rank approximation are referred to in this

thesis. Shanmugan's book [37] was used as a reference for random signal principles. His definition of correlation coefficient, along with other random signal principles, is applied in this study.

An article by Buckley and Griffiths [6] about an adaptive GSC with derivative constraints was useful. It pointed out that when using derivative constraints the quiescent beampattern depends on the location of the phase center of the array. This information helped to solve a problem encountered when applying eigenvector constraints to an adaptive GSC. Er and Cantoni [13] also wrote an article on derivative constraints for broadband, element space, array processors. In all the arrays they analyzed, the phase center of the array was chosen as the zero phase reference.

Frost [15] first wrote about the use of linear constraints for the time domain, element space processors, on which the beamformers in this thesis are based. He includes a lot of the mathematics missing from the other articles. He also provides a detailed geometrical interpretation of the linearly constrained minimum variance (LCMV) problem. Er and Cantoni [14] discuss a broadband processor without pre-steering time delays, which are required by the Frost processor. Griffiths and Jim first described the GSC approach to LCMV beamforming in their article [21]. Jablon [23] also discussed the GSC and evaluated its steady state cancellation performance.

Adaptive arrays typically have main lobe and sidelobe shapes differing from those designed from deterministic, nonadaptive arrays. Three articles present procedures for approximating a desired quiescent beampattern with a partially adaptive beamformer. Two of the articles [20][19] discuss a method based on the use of the GSC. Both of these methods require one additional linear constraint for both narrowband and broadband arrays. Van Veen [43] describes a method to approximate the desired response which uses any or all of the available degrees of freedom.

Partially adaptive beamformer designs are analyzed and evaluated in several sources. Van Veen [40] mentions two design methods for partially adaptive broadband beamformers: the eigenstructure based and the power minimization based design procedures. The eigenstructure based design [42][40] problem is simpler to solve than the power minimization problem, but requires more

adaptive weights for comparable performance. Power minimization based design [46][41][39] gives the best interference cancellation performance with the fewest weights. It is helpful to read Liu and Van Veen's [26] article to better understand the power minimization based design. Van Veen [39] explains that beam based designs are not justified for broadband systems. Partially adaptive beamforming is out of scope in this thesis, but would be the next logical extension to the fully adaptive case examined here.

Van Veen [44] wrote about soft response constraints with minimum variance beamformers. LCMV beamformers use hard constraints to control the response of the desired signal. If the constraint is allowed to permit distortion of the desired signal, the interference cancellation performance can be improved. Van Veen's approach is to minimize the variance subject to a constraint on the mean-square response (quadratic constraint on the weights).

Several articles describe coherent and correlated narrowband signals. Li and Chang [25] modeled a narrowband multipath signal as a scaled and delayed version of a direct path signal. The narrowband multipath scenario generated in this work is based on this model. Reddy [34] describes a narrowband model for two coherent sources. Shan [36] and Godara [17] also cover narrowband models for two or more coherent sources. The correlated narrowband signals generated in this thesis are based on these coherent signal models.

Vural compares the different types of adaptive array processors [47]; the time domain, element space processor is the type considered in this study. Adaptive Technology, Inc. [29] studied the radome multipath reflection problem. Their report covers the problem and possible solutions. The idea to model the radome as two flat plates originated from this report.

III. Preliminaries

3.1 Introduction

A beamformer weights and sums data from an array of sensor elements to perform spatial filtering. Spatial filtering involves separating signals which have similar temporal frequency content but arrive from different directions. Signals are classified as either narrowband or broadband. One definition of narrowband is in terms of the fractional bandwidth. The fractional bandwidth is the signal bandwidth as a percentage of the carrier frequency. Signals with fractional bandwidths much less than 1% are classified as narrowband and those with fractional bandwidths much greater than 1% are broadband [40]. Another definition of narrowband is in terms of the time bandwidth product (TBWP). The TBWP is the product of two terms: 1) the temporal aperture or the time it takes a wave to propagate from the first to the last sensor and through the taps and 2) the bandwidth of the signal. Signals with a TBWP much less than one are considered narrowband and those with a TBWP much greater than one are broadband [40]. A narrowband beamformer is analogous to a finite impulse response (FIR) filter. While the response of a FIR filter is a function of frequency, a beamformer's response is a function of both angle of arrival and frequency. Narrowband beamformers are much easier to analyze than broadband and will be developed first. The broadband beamformer will be described second. The beamformers are designed according to the linearly constrained, minimum variance form.

3.2 Basic Definitions

Vectors and matrices are used throughout this thesis. Vectors are denoted by bold face lower case symbols, and are assumed to be column vectors. Matrices are denoted by upper case symbols. In this thesis, A^* , A^H and A^{-1} denote the operations of complex conjugate, Hermitian or complex conjugate transpose, and inverse of a matrix A , respectively.

3.3 Basic Concepts

3.3.1 Narrowband Beamforming. Figure 3.1 is a schematic for a narrowband beamformer. It essentially weights and sums the data at the sensors and, accordingly, is sometimes called a weighted delay-and-sum beamformer [11]. The arrow pointing to the array from an angle θ with respect to the array broadside (perpendicular to the array) represents a plane wave from a source in the far field. Plane wave propagation implies that the wave amplitude is constant at all points

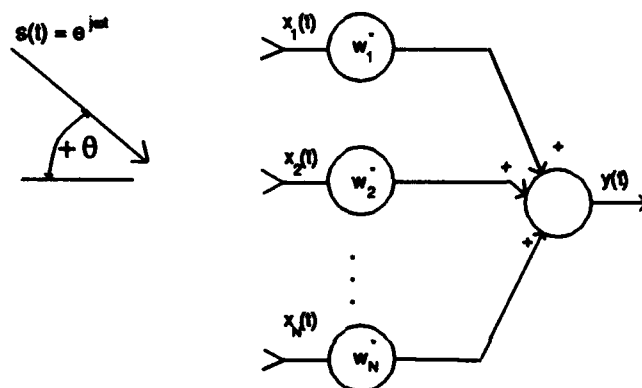


Figure 3.1 Narrowband beamformer

on a line perpendicular to the direction of travel. The beamformer response can therefore be characterized only by delays between sensors, and not amplitude. The elements impart a sampling in space as the wave propagates through the array. The antenna outputs are assumed to have been sampled in time. The number of sensors is chosen to meet the Nyquist criterion for spatial sampling, which implies

$$d \leq \frac{c}{2 \cdot f_{\max}} = \frac{\lambda_{\min}}{2}, \quad (3.1)$$

where c is the speed of propagation in the medium of interest, d is the spacing between elements, f_{\max} is the maximum frequency allowed for the sources, and λ_{\min} is the wavelength corresponding

to f_{\max} . All examples in this thesis use normalized frequency as expressed by

$$-\pi \leq \omega \leq \pi. \quad (3.2)$$

Further, c and d are often normalized to one. To meet the Nyquist criteria for space and time we require $f_{\max} = 1/2$ or $\lambda_{\min} = 2$.

As shown in Figure 3.1, the output of the array at time t is

$$y(t) = \sum_{p=1}^N w_p^* x_p(t), \quad (3.3)$$

where N is the number of antenna elements. A compact vector form of this equation is

$$y(t) = \mathbf{w}^H \mathbf{x}(t), \quad (3.4)$$

where the data at the sensors are represented as

$$\mathbf{x}(t) = [x_1(t) \ x_2(t) \ \cdots \ x_N(t)]^T, \quad (3.5)$$

and the weight vector is

$$\mathbf{w} = [w_1 \ w_2 \ \cdots \ w_N]^T. \quad (3.6)$$

Assume the signal propagating toward the array is a complex sinusoid with direction of arrival (DOA) θ and radian frequency ω . The zero phase reference is taken to be the center of the array. This point need not coincide with a physical antenna element. The data in the p th antenna channel due to a unit amplitude, complex sinusoid in the far field is

$$x_p(t) = e^{j\omega[t + \Delta_p(\theta)]}, \quad 1 \leq p \leq N, \quad (3.7)$$

where $\Delta_p(\theta)$ represents the additional path length in the direction of propagation from the zero phase reference to the p th sensor:

$$\Delta_p(\theta) = \left(\frac{N+1}{2} - p \right) \frac{d \sin \theta}{c}. \quad (3.8)$$

Substituting this into equation 3.3 gives

$$\begin{aligned} y(t) &= \sum_{p=1}^N w_p^* e^{j\omega[t + \Delta_p(\theta)]} \\ &= e^{j\omega t} \sum_{p=1}^N w_p^* e^{j\omega \Delta_p(\theta)} \\ &= e^{j\omega t} \sum_{p=1}^N w_p^* e^{j\omega \left(\frac{N+1}{2} - p \right) \frac{d \sin \theta}{c}} \\ &= e^{j\omega t} r(\theta, \omega), \end{aligned} \quad (3.9)$$

where $r(\theta, \omega)$ is the beamformer response. The response can be expressed in vector notation as

$$r(\theta, \omega) = \mathbf{w}^H \mathbf{d}(\theta, \omega). \quad (3.10)$$

Here $\mathbf{d}(\theta, \omega)$ is the array response vector defined by

$$\mathbf{d}(\theta, \omega) = e^{j\omega \frac{d}{c} \left(\frac{N-1}{2} \right) \sin \theta} \begin{bmatrix} 1 \\ e^{-j\omega \frac{d}{c} \sin \theta} \\ \vdots \\ e^{-j(N-1)\omega \frac{d}{c} \sin \theta} \end{bmatrix}. \quad (3.11)$$

By defining the the vector

$$\mathbf{z}_N(z) = \begin{bmatrix} z^0 \\ z^1 \\ \vdots \\ z^{N-1} \end{bmatrix}, \quad (3.12)$$

Equation 3.11 can be written more compactly as

$$\mathbf{d}(\theta, \omega) = e^{j\omega \frac{L}{c} (\frac{N-1}{2}) \sin \theta} \mathbf{z}_N(e^{-j\omega \frac{L}{c} \sin \theta}). \quad (3.13)$$

From equations 3.9 and 3.10, the beamformer output due to an elemental source can be expressed as

$$y(t) = e^{j\omega t} \mathbf{w}^H \mathbf{d}(\theta, \omega). \quad (3.14)$$

Here,

$$\mathbf{x}(t) = e^{j\omega t} \mathbf{d}(\theta, \omega), \quad (3.15)$$

models the data due to an elemental point source of unit amplitude.

The beampattern is defined to be the magnitude squared of the beamformer response. To plot the beampattern, the responses at the angles of interest are needed. The row vector of beamformer responses can be written as

$$\begin{aligned} \mathbf{r}(\omega, \theta) &= \begin{bmatrix} r(\omega, \theta_1) & r(\omega, \theta_2) & \cdots & r(\omega, \theta_N) \end{bmatrix} \\ &= \begin{bmatrix} \mathbf{w}^H \mathbf{d}(\omega, \theta_1) & \mathbf{w}^H \mathbf{d}(\omega, \theta_2) & \cdots & \mathbf{w}^H \mathbf{d}(\omega, \theta_N) \end{bmatrix}. \end{aligned} \quad (3.16)$$

Another way to get the beamformer response is to take the discrete Fourier transform (DFT) of the complex conjugate of the weight vectors. This gives responses at the angles

$$\theta_i = \sin^{-1} \left[\frac{(i-1) c}{\omega d N} \right]; \quad 1 \leq i \leq N. \quad (3.17)$$

To see this, rewrite equation 3.16 as

$$\mathbf{r}(\omega, \theta) = \mathbf{w}^H \begin{bmatrix} \mathbf{d}(\omega, \theta_1) & \mathbf{d}(\omega, \theta_2) & \dots & \mathbf{d}(\omega, \theta_N) \end{bmatrix}. \quad (3.18)$$

Substituting the array response vectors into equation 3.18 yields

$$\mathbf{r}(\omega, \theta) = \mathbf{w}^H \begin{bmatrix} 1 & 1 & \dots & 1 \\ e^{-j\omega \frac{d}{c} \sin \theta_1} & e^{-j\omega \frac{d}{c} \sin \theta_2} & \dots & e^{-j\omega \frac{d}{c} \sin \theta_N} \\ \vdots & \vdots & \vdots & \vdots \\ e^{-j\omega \frac{d}{c} (N-1) \sin \theta_1} & e^{-j\omega \frac{d}{c} (N-1) \sin \theta_2} & \dots & e^{-j\omega \frac{d}{c} (N-1) \sin \theta_N} \end{bmatrix} D, \quad (3.19)$$

where D is the diagonal matrix

$$D = \text{diag}\{e^{j\omega \frac{d}{c} (\frac{N-1}{2}) \sin \theta_1}, e^{j\omega \frac{d}{c} (\frac{N-1}{2}) \sin \theta_2}, \dots, e^{j\omega \frac{d}{c} (\frac{N-1}{2}) \sin \theta_N}\}. \quad (3.20)$$

The matrix in the center of equation 3.19 is similar to the DFT matrix which is given by

$$V = \begin{bmatrix} 1 & 1 & 1 & 1 \\ 1 & e^{-j(1)\frac{2\pi}{N}} & \dots & e^{-j(1)(N-1)\frac{2\pi}{N}} \\ \vdots & \vdots & \vdots & \vdots \\ 1 & e^{-j(N-1)\frac{2\pi}{N}} & \dots & e^{-j(N-1)(N-1)\frac{2\pi}{N}} \end{bmatrix}. \quad (3.21)$$

It is well known that if \mathbf{f} is a column vector, then

$$\mathbf{g}^T = \mathbf{f}^T V \quad (3.22)$$

is the DFT of \mathbf{f}^T . Comparing the matrix in equation 3.19 with the matrix representation of the DFT in equation 3.21, we see that when

$$\theta_i = \sin^{-1} \left[\frac{(i-1) c 2\pi}{\omega d N} \right]; \quad 1 \leq i \leq N, \quad (3.23)$$

then

$$\mathbf{r}(\omega, \theta) = \mathbf{w}^H V D. \quad (3.24)$$

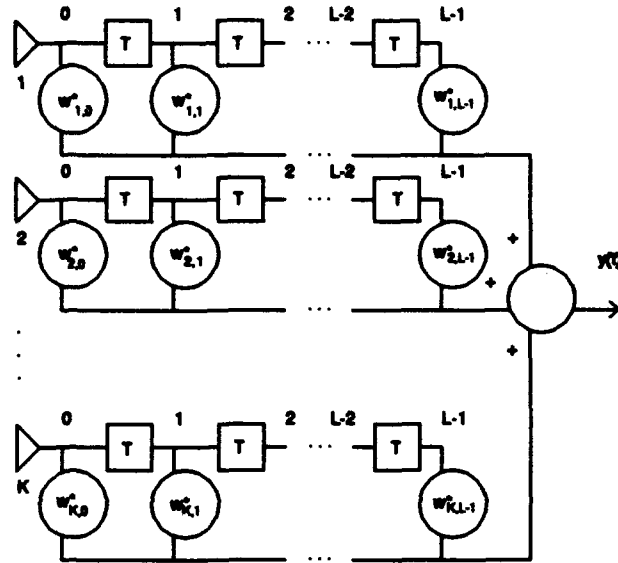


Figure 3.2 Broadband beamformer

3.3.2 Broadband Beamforming. Broadband beamforming is similar to narrowband except that taps are added to allow for interference cancellation over a band of frequencies. The Nyquist criterion for spatial sampling is met as in the narrowband case. The delay between each of the taps is normalized to 1 sec. The Nyquist criterion for temporal sampling is

$$\omega_s = \frac{2\pi}{T} \geq 2\omega_{\max}. \quad (3.25)$$

With T normalized to one second, temporal frequency is normalized as

$$-\pi \leq \omega \leq \pi. \quad (3.26)$$

Figure 3.2 is the schematic for a broadband beamformer. With the broadband beamformer, there is a datum at each of taps. The equation for the output now becomes

$$y(t) = \sum_{p=1}^K \sum_{m=0}^{L-1} w_{p,m}^* x_p(t, m), \quad (3.27)$$

where K is the number of sensors and L is the number of taps. Delayed versions of the data at each sensor can be written as

$$x_p(t, m) = e^{j\omega[t-mT+\Delta_p(\theta)]}, \quad (3.28)$$

where m ranges from 0 to $L-1$ and T is the time delay between adjacent taps illustrated in Figure 3.2. The zero phase reference is at the center of the array as in the narrowband case. Substituting the above equation into equation 3.27 gives

$$\begin{aligned} y(t) &= \sum_{p=1}^K \sum_{m=0}^{L-1} w_{p,m}^* e^{j\omega t} e^{-j\omega[mT-\Delta_p(\theta)]} \\ &= e^{j\omega t} \sum_{p=1}^K \sum_{m=0}^{L-1} w_{p,m}^* e^{-j\omega[mT-\Delta_p(\theta)]} \\ &= e^{j\omega t} \sum_{p=1}^K \sum_{m=0}^{L-1} w_{p,m}^* e^{-j\omega mT} e^{j\omega \Delta_p(\theta)} \\ &= e^{j\omega t} \sum_{p=1}^K \sum_{m=0}^{L-1} w_{p,m}^* e^{-j\omega mT} e^{j\omega \left(\frac{K+1}{2}-p\right) \frac{d \sin \theta}{c}} \\ &= e^{j\omega t} r(\theta, \omega). \end{aligned} \quad (3.29)$$

As before, $r(\theta, \omega)$ is the beamformer response. Again, the response can be expressed in vector notation as

$$r(\theta, \omega) = \mathbf{w}^H \mathbf{d}(\theta, \omega), \quad (3.30)$$

where $\mathbf{d}(\theta, \omega)$ is now expressed as

$$\mathbf{d}(\theta, \omega) = e^{j\omega \frac{d}{c} (\frac{K+1}{2}) \sin \theta} \begin{bmatrix} e^{-j\omega(1)\frac{d}{c} \sin \theta} \\ e^{-j\omega(2)\frac{d}{c} \sin \theta} \\ \vdots \\ e^{-j\omega(K)\frac{d}{c} \sin \theta} \\ \vdots \\ e^{-j\omega(1)T} e^{-j\omega(1)\frac{d}{c} \sin \theta} \\ e^{-j\omega(1)T} e^{-j\omega(2)\frac{d}{c} \sin \theta} \\ \vdots \\ e^{-j\omega(1)T} e^{-j\omega(K)\frac{d}{c} \sin \theta} \\ \vdots \\ e^{-j\omega(L-1)T} e^{-j\omega(1)\frac{d}{c} \sin \theta} \\ e^{-j\omega(L-1)T} e^{-j\omega(2)\frac{d}{c} \sin \theta} \\ \vdots \\ e^{-j\omega(L-1)T} e^{-j\omega(K)\frac{d}{c} \sin \theta} \end{bmatrix}, \quad (3.31)$$

and the weight vector is

$$\mathbf{w} = [w_{1,0} \ w_{2,0} \ \cdots \ w_{K,0} \ w_{1,1} \ w_{2,1} \ \cdots \ w_{K,1} \ \cdots \ w_{1,L-1} \ w_{2,L-1} \ \cdots \ w_{K,L-1}]^T. \quad (3.32)$$

This array response vector can be expressed more simply as

$$\mathbf{d}(\theta, \omega) = e^{j\omega \frac{d}{c} (\frac{K+1}{2}) \sin \theta} \mathbf{\Psi}_L(e^{-j\omega T}) \otimes \mathbf{\Psi}_K(e^{-j\omega \frac{d}{c} \sin \theta}), \quad (3.33)$$

where the symbol \otimes is the Kronecker product defined in [27]. An example of a Kronecker product is

$$A \otimes B = \begin{bmatrix} a_{11}B & a_{12}B \\ a_{21}B & a_{22}B \end{bmatrix}, \quad (3.34)$$

where

$$A = \begin{bmatrix} a_{11} & a_{12} \\ a_{21} & a_{22} \end{bmatrix},$$

and B is a matrix. For the broadband case, we evaluate the beamformer response as a function of both angle and frequency. Therefore, we define the beamformer response matrix as

$$H(\omega, \theta) = \begin{bmatrix} \mathbf{w}^H \mathbf{d}(\omega_1, \theta_1) & \mathbf{w}^H \mathbf{d}(\omega_1, \theta_2) & \cdots & \mathbf{w}^H \mathbf{d}(\omega_1, \theta_N) \\ \mathbf{w}^H \mathbf{d}(\omega_2, \theta_1) & \mathbf{w}^H \mathbf{d}(\omega_2, \theta_2) & \cdots & \mathbf{w}^H \mathbf{d}(\omega_2, \theta_N) \\ \vdots & \vdots & \vdots & \vdots \\ \mathbf{w}^H \mathbf{d}(\omega_N, \theta_1) & \mathbf{w}^H \mathbf{d}(\omega_N, \theta_2) & \cdots & \mathbf{w}^H \mathbf{d}(\omega_N, \theta_N) \end{bmatrix}. \quad (3.35)$$

This equation may be solved directly for the response. However, as in the narrowband case, an alternate method exists for calculating the response. If the stacked weight vector is unstacked and put into matrix form, the DFT of the rows and columns can be used to obtain the beampattern. The concept is the same as in the narrowband case except a DFT is performed on each row (corresponding to different frequencies), and then to each column (corresponding to different angles), of the beamformer response matrix. This case is more complicated than narrowband since the angular spacing is different from frequency to frequency. At each frequency, the number of valid points must be calculated.

3.4 Data Generation

All the data used in this thesis are simulated. Since the data are assumed WSS, the covariance matrix of \mathbf{x} can be written as

$$R_{xx} = E[\mathbf{x}\mathbf{x}^H]. \quad (3.36)$$

In the narrowband case, the data covariance matrix for a narrowband signal at frequency ω_o is represented as

$$R_{xx} = \sigma^2 \mathbf{d}(\theta_s, \omega_o) \mathbf{d}^H(\theta_s, \omega_o) + R_{nn}, \quad (3.37)$$

where σ^2 is the power or variance of the signal, θ_s is the DOA of the source, ω_o is the radian frequency of the signal, and R_{nn} is the covariance matrix of the noise. When the signal originates from a single DOA but is broadband, the expression becomes

$$R_{xx} = \frac{1}{2\pi} \int_{\omega \in \Omega} S(\omega) \mathbf{d}(\theta, \omega) \mathbf{d}^H(\theta, \omega) d\omega + R_{nn}, \quad (3.38)$$

where $S(\omega)$ is a weighting function over frequency, called the power spectral density (PSD), and Ω is the frequency extent of the source. The most general expression is

$$R_{xx} = \frac{1}{2\pi} \int_{\theta \in \Theta} \int_{\omega \in \Omega} S(\theta, \omega) \mathbf{d}(\theta_s, \omega) \mathbf{d}^H(\theta, \omega) d\omega d\theta + R_{nn}, \quad (3.39)$$

where $S(\theta, \omega)$ is a weighting over frequency and DOA and is also a PSD, and Θ is the spatial extent of the source. The noise is assumed to be additive and white. It is assumed Gaussian with covariance $\sigma_n^2 I$, where σ_n^2 is the white noise power and I is the identity matrix.

3.5 Linear Constraint Design

The simplest type of constraint is that of a point constraint, which constrains the beamformer response at a specified frequency and DOA. The response is constrained at radian frequency ω_o and angle θ_s as

$$\mathbf{w}^H \mathbf{d}(\theta_s, \omega_o) = r, \quad (3.40)$$

where r is the desired complex response. Several linear constraints can be expressed as

$$\mathbf{C}^H \mathbf{w} = \mathbf{g}, \quad (3.41)$$

where \mathbf{C} is the constraint matrix and \mathbf{g} the response vector. The matrix \mathbf{C} is chosen to contain M linear constraints so the above equation represents M linearly independent columns in N unknowns. The weight vector \mathbf{w} has length N , where in the broadband case $N = K \times L$. This makes the dimensions of \mathbf{C} , N by M . If $N = M$, then \mathbf{w} is uniquely determined by the constraints. To ensure there is a \mathbf{w} which satisfies the constraints, M is chosen to be less than N . An example of multiple point constraints is

$$[\mathbf{d}(\theta_{s1}, \omega_o) \ \mathbf{d}(\theta_{s2}, \omega_o) \ \mathbf{d}(\theta_{s3}, \omega_o)]^H \mathbf{w} = [r_1 \ r_2 \ r_3]^T. \quad (3.42)$$

In this case, $M = 3$, $\mathbf{C} = [\mathbf{d}(\theta_{s1}, \omega_o) \ \mathbf{d}(\theta_{s2}, \omega_o) \ \mathbf{d}(\theta_{s3}, \omega_o)]$, and $\mathbf{g} = [r_1 \ r_2 \ r_3]^T$.

A more efficient type of constraint in the broadband case is the eigenvector constraint. Eigenvector constraints are used to approximate a desired broadband response using only a few linear constraints.

3.6 Linearly Constrained Minimum Variance (LCMV) Beamforming

3.6.1 LCMV Criterion. The LCMV criterion applies to both narrowband and broadband beamforming. The objective is to pass a desired signal while minimizing power from undesired signals. This is accomplished by constraining the beamformer response in a desired direction while minimizing the output power or variance. The problem to be solved is

$$\min_{\mathbf{w}} P_o \text{ subject to } C^H \mathbf{w} = \mathbf{g}. \quad (3.43)$$

P_o is the expected value of the output power and is expressed as

$$P_o = E[|y|^2] = E[yy^H] = \mathbf{w}^H E[\mathbf{x}\mathbf{x}^H] \mathbf{w}. \quad (3.44)$$

Thus, the problem is restated as

$$\min_{\mathbf{w}} \mathbf{w}^H R_{xx} \mathbf{w} \text{ subject to } C^H \mathbf{w} = \mathbf{g}. \quad (3.45)$$

To begin to solve this problem, guess that the solution is

$$\mathbf{w}_g = R_{xx}^{-1} C [C^H R_{xx}^{-1} C]^{-1} \mathbf{g}. \quad (3.46)$$

Equation 3.46 is a valid guess because C is full rank and R_{xx} is positive definite (this ensures the inverses exist) [40]. Other solutions of the form $\mathbf{w} = \mathbf{w}_g + \mathbf{a}$ meet the constraint so long as $C^H \mathbf{a} = 0$. Substituting this solution back in the objective function gives

$$\begin{aligned} \mathbf{w}^H R_{xx} \mathbf{w} &= (\mathbf{w}_g^H + \mathbf{a}^H) R_{xx} (\mathbf{w}_g + \mathbf{a}) \\ &= \mathbf{w}_g^H R_{xx} \mathbf{w}_g + \mathbf{w}_g^H R_{xx} \mathbf{a} + \mathbf{a}^H R_{xx} \mathbf{w}_g + \mathbf{a}^H R_{xx} \mathbf{a} \\ &= \mathbf{w}_g^H R_{xx} \mathbf{w}_g + \mathbf{g}^H [C^H R_{xx}^{-1} C]^{-1} C^H R_{xx}^{-1} R_{xx} \mathbf{a} + \mathbf{a}^H R_{xx} R_{xx}^{-1} C [C^H R_{xx}^{-1} C]^{-1} \mathbf{g} + \mathbf{a}^H R_{xx} \mathbf{a} \end{aligned}$$

$$\begin{aligned}
&= \mathbf{w}_j^H \mathbf{R}_{xx} \mathbf{w}_j + \mathbf{g}^H [\mathbf{C}^H \mathbf{R}_{xx}^{-1} \mathbf{C}]^{-1} \mathbf{C}^H \mathbf{a} + \mathbf{a}^H \mathbf{C} [\mathbf{C}^H \mathbf{R}_{xx}^{-1} \mathbf{C}]^{-1} \mathbf{g} + \mathbf{a}^H \mathbf{R}_{xx} \mathbf{a} \\
&= \mathbf{w}_j^H \mathbf{R}_{xx} \mathbf{w}_j + \mathbf{a}^H \mathbf{R}_{xx} \mathbf{a},
\end{aligned} \tag{3.47}$$

since $\mathbf{C}^H \mathbf{a} = 0$. We see that all other possible solutions which do not violate the constraint make the objective function larger. Thus, \mathbf{w}_j gives a minimum.

3.6.2 Generalized Sidelobe Canceller. The generalized sidelobe canceller (GSC) is another equivalent form of the LCMV beamformer. Figure 3.3 is the schematic of the GSC implementation of the LCMV beamformer. The derivation that follows is from Van Veen [40].

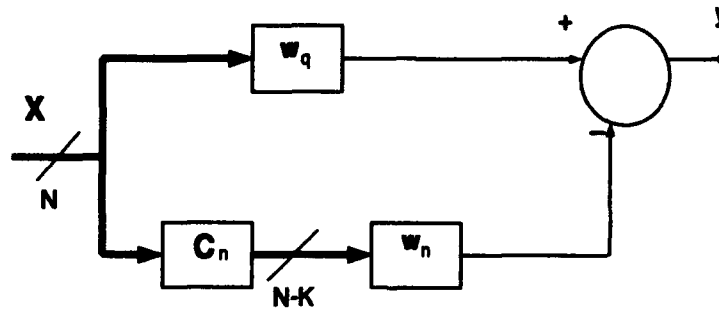


Figure 3.3 Generalized sidelobe canceller schematic

The GSC uses an orthogonal basis for the null space of the constraint matrix \mathbf{C} . Form the matrix \mathbf{C}_n as the orthogonal complement to the space spanned by the columns of the full rank constraint matrix \mathbf{C} . \mathbf{C}_n is size N by $N - M$. Together the columns of \mathbf{C} and \mathbf{C}_n span the entire N dimensional space. The weight vector can be expressed in terms of a set of basis vectors as

$$\mathbf{w} = \mathbf{C}\mathbf{v} - \mathbf{C}_n \mathbf{w}_n, \tag{3.48}$$

where \mathbf{v} is M by 1 and \mathbf{w}_n is $N - M$ by 1. $C\mathbf{v}$ and $C_n\mathbf{w}_n$ represent the components of \mathbf{w} in the spaces spanned by the columns of C and C_n , respectively. Since the columns of C_n and C are orthogonal, $C^H C_n = 0$. Applying the constraint to this new weight vector gives

$$C^H \mathbf{w} = C^H C \mathbf{v} - C^H C_n \mathbf{w}_n = C^H C \mathbf{v}. \quad (3.49)$$

Using the linear constraint equations from equation 3.43, \mathbf{v} can be expressed as

$$\mathbf{v} = (C^H C)^{-1} \mathbf{g}. \quad (3.50)$$

Substituting this back in equation 3.48 results in

$$\mathbf{w} = C(C^H C)^{-1} \mathbf{g} - C_n \mathbf{w}_n. \quad (3.51)$$

The first term in the above equation only depends on the constraints and is independent of the data. This part is implemented in the upper branch of the GSC and represents a nonadaptive beamformer. The first term in equation 3.51 is sometimes called the quiescent weight since it is the part independent of the data. It is represented as

$$\mathbf{w}_q = C(C^H C)^{-1} \mathbf{g}. \quad (3.52)$$

The lower branch of the GSC consists of an unconstrained adaptive beamformer. The number of adaptive weights is $N - M$. The constraint matrix C preserves the desired signal. Thus, the matrix C_n blocks the component of the data that lies in the space spanned by the columns of C . For this reason, C_n is referred to as the signal blocking matrix.

Using the GSC, the LCMV problem is expressed as the unconstrained problem

$$\min_{\mathbf{w}_n} (\mathbf{w}_q - C_n \mathbf{w}_n)^H R_{xx} (\mathbf{w}_q - C_n \mathbf{w}_n). \quad (3.53)$$

The solution [40] to this equation is

$$\mathbf{w}_n = (C_n^H R_{xx} C_n)^{-1} C_n^H R_{xx} \mathbf{w}_q. \quad (3.54)$$

The reason to implement this form is that the direct form LCMV beamformer requires a constrained adaptive algorithm, which is more complex than an unconstrained one.

IV. Analysis and Simulations

4.1 Introduction

This chapter applies concepts from chapter 3 to the simplified RMR problem. Before the actual problem is addressed, basic narrowband and broadband beamforming concepts are tested and compared to results in the literature. Since the implementation of the guiding equations and algorithms were not revealed in the articles, the developments are included here. Much time will be saved by using these derivations and algorithms in the future. The actual algorithms are written using Matlab. The files are included in the appendix.

4.2 Narrowband Beamforming

4.2.1 Data Generation.

4.2.1.1 Uncorrelated Sources. Complex data are generated for the narrowband case. The covariance of a single narrowband source is represented [24] as

$$R_s = \sigma_s^2 \mathbf{d}(\theta_s, \omega_s) \mathbf{d}(\theta_s, \omega_s)^H. \quad (4.1)$$

Here the data \mathbf{x} are generated as a random amplitude times the array response vector. For two uncorrelated sources this becomes

$$\begin{aligned} \mathbf{x} &= \mathbf{s} + \mathbf{n} \\ &= a_1 \mathbf{d}_1 + a_2 \mathbf{d}_2 + \mathbf{n}, \end{aligned} \quad (4.2)$$

where \mathbf{s} is the received signal vector, the a_i 's are random signal amplitudes, and the \mathbf{d}_i 's are array response vectors. This equation can be represented as

$$\mathbf{x} = B\mathbf{a} + \mathbf{n}, \quad (4.3)$$

where $\mathbf{a} = [a_1 \ a_2]^T$, $B = [\mathbf{d}_1 \ \mathbf{d}_2]$, and \mathbf{n} is uncorrelated noise represented as $[n_1 \ n_2]^T$. The vector \mathbf{a} is sometimes called the signal-in-space vector [24]. Assume a_1 and a_2 are statistically independent and the vectors \mathbf{a} and \mathbf{n} are independent and normally distributed with zero mean. Further, \mathbf{n} is Gaussian with covariance $\sigma^2 I$. The data covariance matrix can be computed as

$$\begin{aligned} R_{xx} &= E[\mathbf{x}\mathbf{x}^H] \\ &= E[(B\mathbf{a} + \mathbf{n})(\mathbf{a}^H B^H + \mathbf{n}^H)] \\ &= E[B\mathbf{a}\mathbf{a}^H B^H] + E[\mathbf{n}\mathbf{a}^H B^H] + E[B\mathbf{a}\mathbf{n}^H] + E[\mathbf{n}\mathbf{n}^H] \\ &= BE[\mathbf{a}\mathbf{a}^H]B^H + R_{nn} \\ &= BR_{aa}B^H + R_{nn} \\ &= R_{ss} + R_{nn}, \end{aligned} \quad (4.4)$$

where R_{ss} is the spatial correlation matrix of the signal and $R_{nn} = \sigma_n^2 I_N$ with I_N the identity matrix of size N . The matrix R_{aa} is the spatial correlation matrix of the signal-in-space vector and is expressed as

$$\begin{aligned} R_{aa} &= E[\mathbf{a}\mathbf{a}^H] \\ &= E \begin{bmatrix} a_1 a_1^* & a_1 a_2^* \\ a_2 a_1^* & a_2 a_2^* \end{bmatrix} \\ &= \begin{bmatrix} E[a_1 a_1^*] & E[a_1 a_2^*] \\ E[a_2 a_1^*] & E[a_2 a_2^*] \end{bmatrix} \end{aligned}$$

$$\begin{aligned}
&= \begin{bmatrix} \sigma_1^2 & 0 \\ 0 & \sigma_2^2 \end{bmatrix} \\
&= \begin{bmatrix} p_1 & 0 \\ 0 & p_2 \end{bmatrix}, \tag{4.5}
\end{aligned}$$

where $E[\mathbf{a}_i \mathbf{a}_i^*] = E[|\mathbf{a}_i|^2] = \sigma_i^2 = p_i$. Notice that R_{xx} can be expressed as

$$\begin{aligned}
R_{xx} &= B \begin{bmatrix} \sigma_1^2 & 0 \\ 0 & \sigma_2^2 \end{bmatrix} B^H + R_{nn} \\
&= [\mathbf{d}_1 \ \mathbf{d}_2] \begin{bmatrix} \sigma_1^2 & 0 \\ 0 & \sigma_2^2 \end{bmatrix} \begin{bmatrix} \mathbf{d}_1^H \\ \mathbf{d}_2^H \end{bmatrix} + R_{nn} \\
&= [\sigma_1^2 \mathbf{d}_1 \ \sigma_2^2 \mathbf{d}_2] \begin{bmatrix} \mathbf{d}_1^H \\ \mathbf{d}_2^H \end{bmatrix} + R_{nn} \\
&= \sigma_1^2 \mathbf{d}_1 \mathbf{d}_1^H + \sigma_2^2 \mathbf{d}_2 \mathbf{d}_2^H \\
&= R_{s1} + R_{s2} + R_{nn}. \tag{4.6}
\end{aligned}$$

This is an expected result for uncorrelated sources.

4.2.1.2 Correlated Sources. Godara [17] represents two correlated signals as

$$\mathbf{s} = \sqrt{p_1} a_1 \mathbf{d}_1 + \sqrt{p_2} (\rho_c^* a_1 + \sqrt{1 - |\rho_c|^2} a_2) \mathbf{d}_2, \tag{4.7}$$

where a_1 and a_2 are independent and have zero mean and unit variance. Also, p_1 and p_2 are the powers of signals one and two, respectively. In the correlated model, the off diagonal elements of R_{aa} are proportional to the correlation coefficient. The correlation coefficient [37] is defined as

$$\rho_c = \frac{E[a_1 a_2^*]}{\sqrt{E[a_1 a_1^*] E[a_2 a_2^*]}}. \tag{4.8}$$

This can be rearranged as

$$E[a_1 a_2^*] = \rho_c \sqrt{p_1 p_2} . \quad (4.9)$$

The matrix R_{aa} is Hermitian symmetric so

$$E[a_2 a_1^*] = \rho_c^* \sqrt{p_1 p_2} . \quad (4.10)$$

Now, compute the data covariance matrix with the R_{aa} as above:

$$\begin{aligned} R_{xx} &= [d_1 \ d_2] \begin{bmatrix} p_1 & \rho_c \sqrt{p_1 p_2} \\ \rho_c^* \sqrt{p_1 p_2} & p_2 \end{bmatrix} \begin{bmatrix} d_1^H \\ d_2^H \end{bmatrix} + R_{nn} \\ &= [p_1 d_1 + \rho_c^* d_2 \sqrt{p_1 p_2} \quad \rho_c d_1 \sqrt{p_1 p_2} + d_2 p_2] \begin{bmatrix} d_1^H \\ d_2^H \end{bmatrix} + R_{nn} \\ &= p_1 d_1 d_1^H + \rho_c^* d_2 \sqrt{p_1 p_2} d_1^H + \rho_c d_1 \sqrt{p_1 p_2} d_2^H + p_2 d_2 d_2^H + R_{nn} . \end{aligned} \quad (4.11)$$

4.2.1.3 Multipath Model. The multipath model used simulates a specular, single bounce reflection off a flat plate into the antenna array. Figure 4.1 shows the set up. The plate on the right does not reflect energy; signals pass through unaffected. Signals from positive DOAs reflect off the left plate according to

$$\rho_r(\theta) = \frac{\theta^2}{(\frac{\pi}{2})^2} u(\theta), \quad (4.12)$$

where $\rho_r(\theta)$ is the reflection coefficient, $u(\theta)$ is the unit step function, and θ is the angle from the broad side of the array in radians. This correlation coefficient function of θ was chosen because it approximates that of an actual radome. When signals arrive at broad side (perpendicular to the array), there are few or no reflections. Signals reflect more as the angle from broad side increases (100 % reflection at 90° from broad side). The reflection process is assumed to only attenuate the

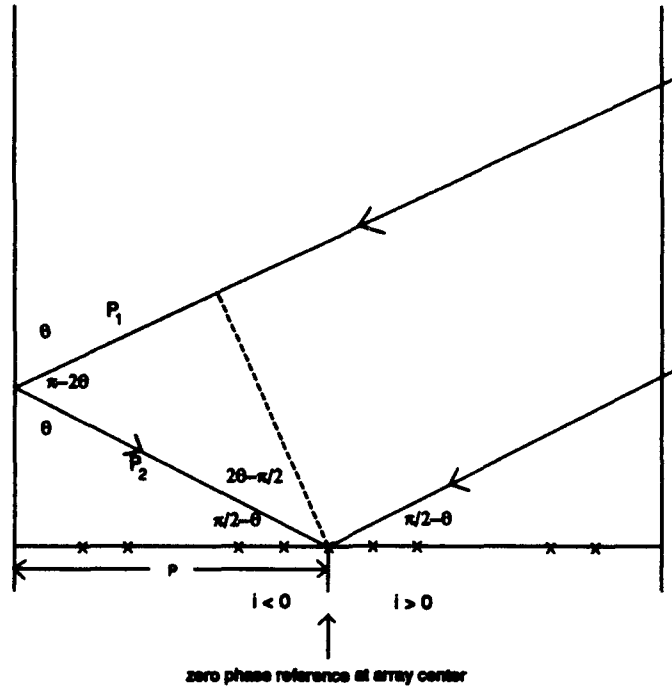


Figure 4.1 Two plate multipath model

signal after it bounces off the plate. No random phase is introduced by the reflection surface; it is assumed to be perfectly smooth. The wave starts out planar and remains that way after it bounces off the wall. The reflected or indirect path wave is modeled as a scaled and delayed version of the direct path wave. For a narrowband signal, the signal part of the data observed by the sensors is given by

$$\begin{aligned}
 s &= a_1 d_1 + a_2 d_2 \\
 &= a_1 d_1 + \rho_r a_1 e^{-j\Phi} d_2 \\
 &= a_1 d_1 + \rho_r a_1 e^{-j\frac{2\pi}{\lambda} \Delta R} d_2,
 \end{aligned} \tag{4.13}$$

where ΔR is the path length difference between the direct path and indirect path wave at the zero phase reference of the array.

The signal covariance matrix for this model is

$$\begin{aligned}
 R_{ss} &= E[ss^H] \\
 &= E[(a_1 d_1 + \rho_r a_1 e^{-j \frac{2\pi}{\lambda} \Delta R} d_2)(a_1^* d_1^H + \rho_r^* a_1^* e^{j \frac{2\pi}{\lambda} \Delta R} d_2^H)] \\
 &= E[a_1 a_1^*] d_1 d_1^H + E[a_1 a_1^*] e^{j \frac{2\pi}{\lambda} \Delta R} \rho_r^* d_1 d_2^H + E[a_1 a_1^*] \rho_r e^{-j \frac{2\pi}{\lambda} \Delta R} d_2 d_1^H + E[a_1 a_1^*] |\rho_r|^2 d_2 d_2^H \\
 &= \sigma_1^2 d_1 d_1^H + \sigma_1^2 e^{j \frac{2\pi}{\lambda} \Delta R} \rho_r^* d_1 d_2^H + \sigma_1^2 \rho_r e^{-j \frac{2\pi}{\lambda} \Delta R} d_2 d_1^H + \sigma_1^2 |\rho_r|^2 d_2 d_2^H. \quad (4.14)
 \end{aligned}$$

The data covariance matrix for the above signal covariance matrix can be written in vector notation as

$$R_{xx} = [d_1 \ d_2] \begin{bmatrix} \sigma_1^2 & \sigma_1^2 \rho_r^* e^{j \frac{2\pi}{\lambda} \Delta R} \\ \sigma_1^2 \rho_r e^{-j \frac{2\pi}{\lambda} \Delta R} & \sigma_1^2 |\rho_r|^2 \end{bmatrix} \begin{bmatrix} d_1^H \\ d_2^H \end{bmatrix} + R_{nn}. \quad (4.15)$$

This gives R_{aa} as

$$R_{aa} = \begin{bmatrix} \sigma_1^2 & \sigma_1^2 \rho_r^* e^{j \frac{2\pi}{\lambda} \Delta R} \\ \sigma_1^2 \rho_r e^{-j \frac{2\pi}{\lambda} \Delta R} & \sigma_1^2 |\rho_r|^2 \end{bmatrix}. \quad (4.16)$$

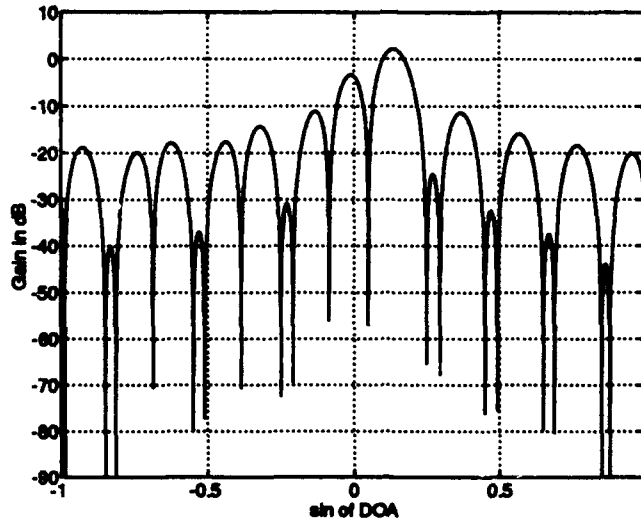


Figure 4.2 Narrowband beamformer with eight interferers; SNR = INR = 60 dB

4.2.2 Point Constraints. Point constraints are used with the narrowband beamformers. In all cases the beamformer response is constrained to unity in the direction of the desired signal. Figure 4.2 displays the beampattern for a beamformer constrained at the DOA $\arcsin(0.1)$ with a signal environment consisting of eight uncorrelated interferers from direction sines of -0.85, -0.55, -0.25, 0.05, 0.25, 0.45, 0.65, and 0.85 in uncorrelated noise. The frequency of all signals is $1/2$ (or $\omega = \pi$). The interferers have power levels 60 db relative to the noise. Figure 4.2 shows this result, which is the same as that obtained by Van Veen [40]. The file `bfnb9s.m` contains the code for this problem. Using the GSC form of the LCMV beamformer provides the same results as the direct form.

The GSC form with point constraints is used for the multipath simulation. The frequency of all signals is again $1/2$ ($\omega = \pi$). The multipath case is set up with the interferer arriving from +45 degrees and reflecting into the desired look direction, which is chosen as -45 degrees. This is the worst case for the multipath in that all the reflected signal will reflect into the main beam. When the interference signal reflects into the main beam, a null formed in the DOA of the

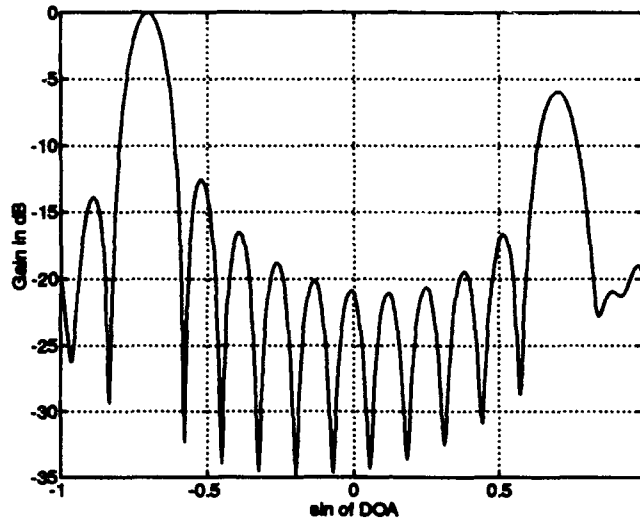


Figure 4.3 Narrowband beampattern for multipath case

interferer will not solve the problem. The beamformer must cancel the direct path signal with the indirect path signal. The more correlated these two signals are, the better they can be cancelled. Since the multipath reflection signal is a scaled and delayed replica of the direct path signal, the two are correlated. The indirect interference signal can be destructively added to the direct path interference signal because they are correlated. Since the reflection coefficient at 45 degrees is $1/4$ (from equation 4.12), the reflected signal is one fourth the amplitude of the direct signal and delayed in time. To cancel these signals, the beamformer forms a beam four times as large in amplitude in the direction of the reflected signal as in the direct path direction (see figure 4.3). Since this is a beampattern plot (magnitude squared), the difference in the beam gains is 12 dB. To see the amount of cancellation, the output power of the beamformer is calculated. This gives the response of the entire system (including plates) to unit amplitude far field sources. Figure 4.4 is the output power of the beamformer with the quiescent weights, while figure 4.5 is the output power with the adapted weights. The Matlab files `outputpownbq.m` and `outputpownbw.m` contain the code to compute and plot the output power. Figure 4.5 shows that the interference signal at 45 degrees has been cancelled.

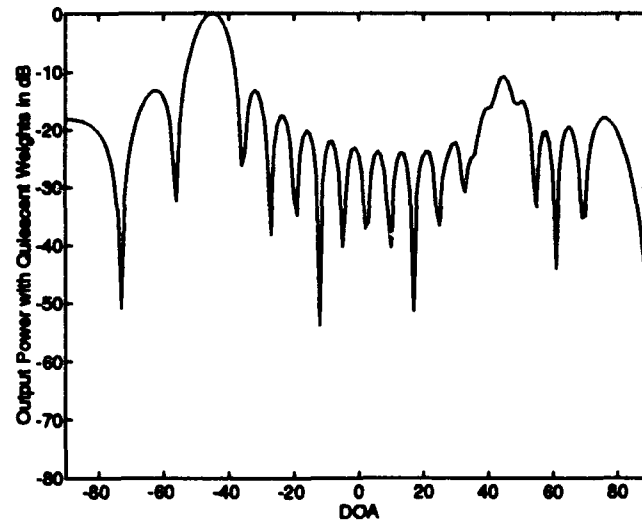


Figure 4.4 Output power with quiescent weights; SNR = 60 dB

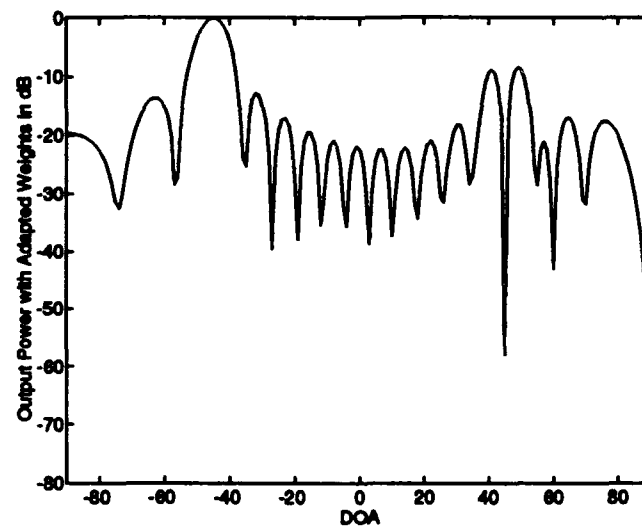


Figure 4.5 Output power with adapted weights

4.3 Broadband Beamforming

4.3.1 Data Generation.

4.3.1.1 *Uncorrelated Sources.* Real data are generated for the broadband case. Constant PSDs are assumed for all sources; this weights all frequencies evenly and is the worst case assumption [40]. The PSD used is

$$S(\omega) = \frac{1}{2}\chi_{[-\omega_b, -\omega_a]}(\omega) + \frac{1}{2}\chi_{[\omega_a, \omega_b]}(\omega), \quad (4.17)$$

where $\chi(\omega)$ is the indicator function defined as

$$\chi_{[x,y]}(\omega) = \begin{cases} 1 & \text{if } x \leq \omega \leq y, \\ 0 & \text{otherwise.} \end{cases} \quad (4.18)$$

As defined earlier, the array response vector is

$$\mathbf{d}(\omega, \theta) = e^{j\omega \frac{K-1}{2} \frac{d}{c} \sin \theta} \mathbf{\Psi}_L(e^{-j\omega T}) \otimes \mathbf{\Psi}_K(e^{-j\omega \frac{d}{c} \sin \theta}). \quad (4.19)$$

Signal covariance matrices for the uncorrelated sources with no spatial extent are calculated as follows:

$$\begin{aligned} R_s &= \frac{1}{2\pi} \int_{-\omega_b}^{-\omega_a} S(\omega) \mathbf{d}(\omega, \theta) \mathbf{d}^H(\omega, \theta) d\omega + \frac{1}{2\pi} \int_{\omega_a}^{\omega_b} S(\omega) \mathbf{d}(\omega, \theta) \mathbf{d}^H(\omega, \theta) d\omega \\ &= \frac{1}{4\pi} \int_{-\omega_b}^{-\omega_a} \mathbf{d}(\omega, \theta) \mathbf{d}^H(\omega, \theta) d\omega + \frac{1}{4\pi} \int_{\omega_a}^{\omega_b} \mathbf{d}(\omega, \theta) \mathbf{d}^H(\omega, \theta) d\omega \\ &= \frac{1}{4\pi} \int_{-\omega_b}^{-\omega_a} [e^{j\omega \frac{K-1}{2} \frac{d}{c} \sin \theta} \mathbf{\Psi}_L(e^{-j\omega T}) \otimes \mathbf{\Psi}_K(e^{-j\omega \frac{d}{c} \sin \theta})] [e^{j\omega \frac{K-1}{2} \frac{d}{c} \sin \theta} \mathbf{\Psi}_L(e^{-j\omega T}) \otimes \mathbf{\Psi}_K(e^{-j\omega \frac{d}{c} \sin \theta})]^H d\omega \\ &\quad + \frac{1}{4\pi} \int_{\omega_a}^{\omega_b} [e^{j\omega \frac{K-1}{2} \frac{d}{c} \sin \theta} \mathbf{\Psi}_L(e^{-j\omega T}) \otimes \mathbf{\Psi}_K(e^{-j\omega \frac{d}{c} \sin \theta})] [e^{j\omega \frac{K-1}{2} \frac{d}{c} \sin \theta} \mathbf{\Psi}_L(e^{-j\omega T}) \otimes \mathbf{\Psi}_K(e^{-j\omega \frac{d}{c} \sin \theta})]^H d\omega \end{aligned}$$

$$\begin{aligned}
&= \frac{1}{4\pi} \int_{-\omega_b}^{-\omega_a} [\Psi_L(e^{-j\omega T}) \Psi_L^H(e^{-j\omega T})] \otimes [\Psi_K(e^{-j\omega \frac{d}{c} \sin \theta}) \Psi_K^H(e^{-j\omega \frac{d}{c} \sin \theta})] d\omega \\
&+ \frac{1}{4\pi} \int_{\omega_a}^{\omega_b} [\Psi_L(e^{-j\omega T}) \Psi_L^H(e^{-j\omega T})] \otimes [\Psi_K(e^{-j\omega \frac{d}{c} \sin \theta}) \Psi_K^H(e^{-j\omega \frac{d}{c} \sin \theta})] d\omega. \quad (4.20)
\end{aligned}$$

The two terms in the Kronecker product can be expressed as

$$\Psi_L(e^{-j\omega T}) \Psi_L^H(e^{-j\omega T}) = \begin{bmatrix} 1 & e^{j(1)\omega T} & \dots & e^{j(L-1)\omega T} \\ e^{-j(1)\omega T} & 1 & \dots & e^{j(L-2)\omega T} \\ \vdots & \vdots & \ddots & \vdots \\ e^{-j(L-1)\omega T} & \dots & & 1 \end{bmatrix} \equiv A(\omega) \quad (4.21)$$

and

$$\begin{aligned}
\Psi_K(e^{-j\omega \frac{d}{c} \sin \theta}) \Psi_K^H(e^{-j\omega \frac{d}{c} \sin \theta}) &= \begin{bmatrix} 1 & e^{j(1)\omega \frac{d}{c} \sin \theta} & \dots & e^{j(K-1)\omega \frac{d}{c} \sin \theta} \\ e^{-j(1)\omega \frac{d}{c} \sin \theta} & 1 & \dots & e^{j(K-2)\omega \frac{d}{c} \sin \theta} \\ \vdots & \vdots & \ddots & \vdots \\ e^{-j(K-1)\omega \frac{d}{c} \sin \theta} & \dots & & 1 \end{bmatrix} \\
&\equiv B(\omega, \theta). \quad (4.22)
\end{aligned}$$

The signal covariance matrix can now be compactly written as

$$R_s = \frac{1}{4\pi} \int_{-\omega_b}^{-\omega_a} A(\omega) \otimes B(\omega, \theta) d\omega + \frac{1}{4\pi} \int_{\omega_a}^{\omega_b} A(\omega) \otimes B(\omega, \theta) d\omega. \quad (4.23)$$

The above matrix can be expressed as

$$R_s = \frac{1}{4\pi} \begin{bmatrix} \int_{-\omega_b}^{-\omega_a} a_0 B(\omega, \theta) d\omega & \int_{-\omega_b}^{-\omega_a} a_1 B(\omega, \theta) d\omega & \dots & \int_{-\omega_b}^{-\omega_a} a_{(L-1)} B(\omega, \theta) d\omega \\ \int_{-\omega_b}^{-\omega_a} a_{-1} B(\omega, \theta) d\omega & \int_{-\omega_b}^{-\omega_a} a_0 B(\omega, \theta) d\omega & \dots & \int_{-\omega_b}^{-\omega_a} a_{(L-2)} B(\omega, \theta) d\omega \\ \vdots & \vdots & \ddots & \vdots \\ \int_{-\omega_b}^{-\omega_a} a_{-(L-1)} B(\omega, \theta) d\omega & \dots & & \int_{-\omega_b}^{-\omega_a} a_0 B(\omega, \theta) d\omega \end{bmatrix}$$

$$+ \frac{1}{4\pi} \begin{bmatrix} \int_{\omega_a}^{\omega_b} a_0 B(\omega, \theta) d\omega & \int_{\omega_a}^{\omega_b} a_1 B(\omega, \theta) d\omega & \cdots & \int_{\omega_a}^{\omega_b} a_{(L-1)} B(\omega, \theta) d\omega \\ \int_{\omega_a}^{\omega_b} a_{-1} B(\omega, \theta) d\omega & \int_{\omega_a}^{\omega_b} a_0 B(\omega, \theta) d\omega & \cdots & \int_{\omega_a}^{\omega_b} a_{(L-2)} B(\omega, \theta) d\omega \\ \vdots & \vdots & \ddots & \vdots \\ \int_{\omega_a}^{\omega_b} a_{-(L-1)} B(\omega, \theta) d\omega & \cdots & \cdots & \int_{\omega_a}^{\omega_b} a_0 B(\omega, \theta) d\omega \end{bmatrix}, \quad (4.24)$$

where $a_{i_1} = e^{j i_1 \omega T}$. The above matrix is block Toeplitz. The entire matrix can be formed by calculating the blocks of the first row and column and creating a Toeplitz matrix. This is done using Matlab. The block on the i_1^{th} principle diagonal of the above matrix is

$$R(i_1) = \int_{-\omega_b}^{-\omega_a} e^{j i_1 \omega T} B(\omega, \theta) d\omega + \int_{\omega_a}^{\omega_b} e^{j i_1 \omega T} B(\omega, \theta) d\omega. \quad (4.25)$$

The elements on the i_2^{th} principle diagonal of $R(i_2)$ are

$$r(i_1, i_2) = \int_{-\omega_b}^{-\omega_a} e^{j i_1 \omega T} e^{j i_2 \omega \frac{d}{c} \sin \theta} d\omega + \frac{1}{4\pi} \int_{\omega_a}^{\omega_b} e^{j i_1 \omega T} e^{j i_2 \omega \frac{d}{c} \sin \theta} d\omega. \quad (4.26)$$

The variable i_1 ranges from $-(L-1)$ to $(L-1)$ in increments of 1. The variable i_2 ranges from $-(K-1)$ to $(K-1)$ in increments of 1. Each element of the signal covariance matrix is in closed form as

$$\begin{aligned} r(i_1, i_2) &= \frac{1}{4\pi} \int_{-\omega_b}^{-\omega_a} e^{j \omega [i_1 T + i_2 \frac{d}{c} \sin \theta]} d\omega + \frac{1}{4\pi} \int_{\omega_a}^{\omega_b} e^{j \omega [i_1 T + i_2 \frac{d}{c} \sin \theta]} d\omega \\ &= \frac{e^{-j \omega_a [i_1 T + i_2 \frac{d}{c} \sin \theta]} - e^{-j \omega_b [i_1 T + i_2 \frac{d}{c} \sin \theta]} + e^{j \omega_b [i_1 T + i_2 \frac{d}{c} \sin \theta]} - e^{j \omega_a [i_1 T + i_2 \frac{d}{c} \sin \theta]}}{4\pi j [i_1 T + i_2 \frac{d}{c} \sin \theta]} \\ &= \frac{\sin[\omega_b T (i_1 T + i_2 \frac{d}{c} \sin \theta)] - \sin[\omega_a T (i_1 T + i_2 \frac{d}{c} \sin \theta)]}{2\pi (i_1 T + i_2 \frac{d}{c} \sin \theta)} \\ &= \frac{\omega_b T \cdot \text{sinc}[\omega_b (i_1 T + i_2 \frac{d}{c} \sin \theta)] - \omega_a T \cdot \text{sinc}[\omega_a (i_1 T + i_2 \frac{d}{c} \sin \theta)]}{2\pi}, \end{aligned} \quad (4.27)$$

with the sinc function defined as

$$\text{sinc}(x) = \frac{\sin(x)}{x}. \quad (4.28)$$

Equation 4.27 is used to compute necessary elements of the signal covariance matrix. The file `mscmnew.m` implements this equation.

Van Veen [39] described another method of computing the signal covariance matrix for two uncorrelated signals at a single location. First, he defined R_s for a single source as

$$R_s = \int_{\Omega} \rho^2(\omega) \mathbf{d}(\omega) \mathbf{d}^H(\omega) d\omega, \quad (4.29)$$

where $\rho^2(\omega)$ is the source PSD and Ω is the source frequency extent. He approximates the above integral by a Riemann sum and avoids integration in the following equation:

$$\begin{aligned} R_s &\approx \sum_{j=1}^J \rho^2(\omega_j) \mathbf{d}(\omega_j) \mathbf{d}^H(\omega_j) \Delta\omega \\ &\approx A \Gamma^2 A^H, \end{aligned} \quad (4.30)$$

where

$$\begin{aligned} A &= [\mathbf{d}(\omega_1) \ \mathbf{d}(\omega_2) \ \cdots \ \mathbf{d}(\omega_J)] \\ \Gamma^2 &= \text{diag}\{\rho^2(\omega_1), \rho^2(\omega_2), \dots, \rho^2(\omega_J)\} \Delta\omega. \end{aligned} \quad (4.31)$$

Now, the two uncorrelated sources and noise can be expressed as

$$R_{xx} \approx [A_1 \ A_2] \begin{bmatrix} \Gamma_1^2 & 0 \\ 0 & \Gamma_2^2 \end{bmatrix} \begin{bmatrix} A_1^H \\ A_2^H \end{bmatrix} + R_{nn}. \quad (4.32)$$

This equation is used for negative and positive frequencies to obtain real data. Note that $\mathbf{d}(-\omega) = \mathbf{d}^*(\omega)$ and $\mathbf{d}^H(-\omega) = \mathbf{d}^{H*}(\omega) = \mathbf{d}^T(\omega)$. Real data are obtained with the following equation:

$$R_{xx} \approx [A_1 \ A_2] \begin{bmatrix} \frac{\Gamma_1^2}{2} & 0 \\ 0 & \frac{\Gamma_2^2}{2} \end{bmatrix} \begin{bmatrix} A_1^H \\ A_2^H \end{bmatrix} + [A_1^* A_2^*] \begin{bmatrix} \frac{\Gamma_1^2}{2} & 0 \\ 0 & \frac{\Gamma_2^2}{2} \end{bmatrix} \begin{bmatrix} A_1^T \\ A_2^T \end{bmatrix} + R_{nn}. \quad (4.33)$$

The file `R_intur.m` computes the signal covariance matrix using this method.

Next, suppose the source has spatial and frequency extent. The PSD function used is

$$S(\omega, \theta) = \frac{1}{2} \chi_{[-\omega_b, -\omega_a]}(\omega) \chi_{[-\theta_b, -\theta_a]}(\theta) + \frac{1}{2} \chi_{[\omega_a, \omega_b]}(\omega) \chi_{[\theta_a, \theta_b]}(\theta). \quad (4.34)$$

In this case, the covariance matrix involves a double integral and is defined by

$$\begin{aligned} R_s &= \frac{1}{2\pi} \int_{-\theta_b}^{-\theta_a} \int_{-\omega_b}^{-\omega_a} S(\omega, \theta) \mathbf{d}(\omega, \theta) \mathbf{d}^H(\omega, \theta) d\omega d\theta + \frac{1}{2\pi} \int_{\theta_a}^{\theta_b} \int_{\omega_a}^{\omega_b} S(\omega, \theta) \mathbf{d}(\omega, \theta) \mathbf{d}^H(\omega, \theta) d\omega d\theta \\ &= \frac{1}{4\pi} \int_{-\theta_b}^{-\theta_a} \int_{-\omega_b}^{-\omega_a} \mathbf{d}(\omega, \theta) \mathbf{d}^H(\omega, \theta) d\omega d\theta + \frac{1}{4\pi} \int_{\theta_a}^{\theta_b} \int_{\omega_a}^{\omega_b} \mathbf{d}(\omega, \theta) \mathbf{d}^H(\omega, \theta) d\omega d\theta \\ &= \frac{1}{4\pi} \int_{-\theta_b}^{-\theta_a} \int_{-\omega_b}^{-\omega_a} [e^{j\omega \frac{K-1}{2} \frac{\Delta}{c} \sin \theta} \Psi_L \otimes \Psi_K] [e^{j\omega \frac{K-1}{2} \frac{\Delta}{c} \sin \theta} \Psi_L \otimes \Psi_K]^H d\omega d\theta \\ &\quad + \frac{1}{4\pi} \int_{\theta_a}^{\theta_b} \int_{\omega_a}^{\omega_b} [e^{j\omega \frac{K-1}{2} \frac{\Delta}{c} \sin \theta} \Psi_L \otimes \Psi_K] [e^{j\omega \frac{K-1}{2} \frac{\Delta}{c} \sin \theta} \Psi_L \otimes \Psi_K]^H d\omega d\theta \\ &= \frac{1}{4\pi} \int_{-\theta_b}^{-\theta_a} \int_{-\omega_b}^{-\omega_a} [\Psi_L \Psi_L^H] \otimes [\Psi_K \Psi_K^H] d\omega d\theta + \frac{1}{4\pi} \int_{\theta_a}^{\theta_b} \int_{\omega_a}^{\omega_b} [\Psi_L \Psi_L^H] \otimes [\Psi_K \Psi_K^H] d\omega d\theta, \quad (4.35) \end{aligned}$$

where the arguments of Ψ_L and Ψ_K have been dropped and are $e^{-j\omega T}$ and $e^{-j\omega \frac{\Delta}{c} \sin \theta}$, respectively.

This can be solved as in section 4.3.1.1. Each element of the signal covariance matrix is in closed form as

$$r(i_1, i_2) = \frac{1}{4\pi} \int_{-\theta_b}^{-\theta_a} \int_{-\omega_b}^{-\omega_a} e^{j\omega [i_1 T + i_2 \frac{\Delta}{c} \sin \theta]} d\omega d\theta + \frac{1}{4\pi} \int_{\theta_a}^{\theta_b} \int_{\omega_a}^{\omega_b} e^{j\omega [i_1 T + i_2 \frac{\Delta}{c} \sin \theta]} d\omega d\theta$$

$$\begin{aligned}
&= \int_{-\theta_0}^{\theta_0} \frac{e^{-j\omega_0[i_1 \cdot T + i_2 \cdot \frac{d}{c} \sin \theta]} - e^{-j\omega_0[i_1 \cdot T + i_2 \cdot \frac{d}{c} \sin \theta]}}{4\pi j[i_1 \cdot T + i_2 \cdot \frac{d}{c} \sin \theta]} d\theta + \int_{\theta_0}^{\theta_0} \frac{e^{j\omega_0[i_1 \cdot T + i_2 \cdot \frac{d}{c} \sin \theta]} - e^{j\omega_0[i_1 \cdot T + i_2 \cdot \frac{d}{c} \sin \theta]}}{4\pi j[i_1 \cdot T + i_2 \cdot \frac{d}{c} \sin \theta]} d\theta \\
&= \int_{\theta_0}^{\theta_0} \frac{e^{-j\omega_0[i_1 \cdot T - i_2 \cdot \frac{d}{c} \sin \theta]} - e^{-j\omega_0[i_1 \cdot T - i_2 \cdot \frac{d}{c} \sin \theta]}}{-4\pi j[i_1 \cdot T - i_2 \cdot \frac{d}{c} \sin \theta]} d\theta + \int_{\theta_0}^{\theta_0} \frac{e^{j\omega_0[i_1 \cdot T + i_2 \cdot \frac{d}{c} \sin \theta]} - e^{j\omega_0[i_1 \cdot T + i_2 \cdot \frac{d}{c} \sin \theta]}}{4\pi j[i_1 \cdot T + i_2 \cdot \frac{d}{c} \sin \theta]} d\theta \\
&= \int_{\theta_0}^{\theta_0} \frac{e^{-j\omega_0[i_1 \cdot T - i_2 \cdot \frac{d}{c} \sin \theta]} - e^{-j\omega_0[i_1 \cdot T - i_2 \cdot \frac{d}{c} \sin \theta]}}{4\pi j[i_1 \cdot T - i_2 \cdot \frac{d}{c} \sin \theta]} d\theta + \int_{\theta_0}^{\theta_0} \frac{e^{j\omega_0[i_1 \cdot T + i_2 \cdot \frac{d}{c} \sin \theta]} - e^{j\omega_0[i_1 \cdot T + i_2 \cdot \frac{d}{c} \sin \theta]}}{4\pi j[i_1 \cdot T + i_2 \cdot \frac{d}{c} \sin \theta]} d\theta \\
&= \int_{\theta_0}^{\theta_0} \left[\frac{e^{-j\omega_0[i_1 \cdot T - i_2 \cdot \frac{d}{c} \sin \theta]} - e^{-j\omega_0[i_1 \cdot T - i_2 \cdot \frac{d}{c} \sin \theta]}}{4\pi j[i_1 \cdot T - i_2 \cdot \frac{d}{c} \sin \theta]} + \frac{e^{j\omega_0[i_1 \cdot T + i_2 \cdot \frac{d}{c} \sin \theta]} - e^{j\omega_0[i_1 \cdot T + i_2 \cdot \frac{d}{c} \sin \theta]}}{4\pi j[i_1 \cdot T + i_2 \cdot \frac{d}{c} \sin \theta]} \right] d\theta \\
&\approx \sum_{j=1}^J \left[\frac{e^{-j\omega_0[i_1 \cdot T - i_2 \cdot \frac{d}{c} \sin \theta]} - e^{-j\omega_0[i_1 \cdot T - i_2 \cdot \frac{d}{c} \sin \theta]}}{4\pi j[i_1 \cdot T - i_2 \cdot \frac{d}{c} \sin \theta]} + \frac{e^{j\omega_0[i_1 \cdot T + i_2 \cdot \frac{d}{c} \sin \theta]} - e^{j\omega_0[i_1 \cdot T + i_2 \cdot \frac{d}{c} \sin \theta]}}{4\pi j[i_1 \cdot T + i_2 \cdot \frac{d}{c} \sin \theta]} \right] \Delta\theta.
\end{aligned} \tag{4.36}$$

The above equation is implemented in Rdb.m. The file Rtdb.m calls the function Rdb.m and computes the entire covariance matrix.

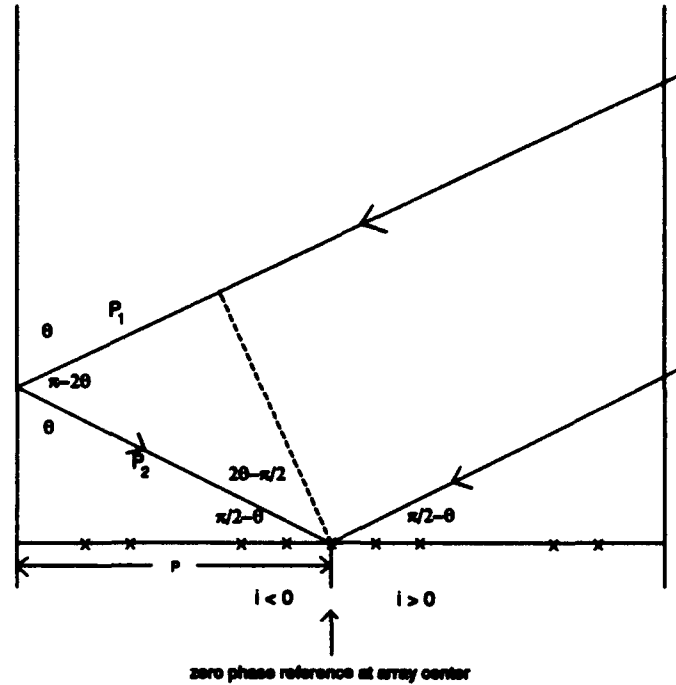


Figure 4.6 Two plate multipath model

4.3.1.2 Multipath Model. Figure 4.6 shows the geometry for the broadband multipath model. It is the same set-up as in section 4.2.1.3 for the narrowband case. The path length difference between the direct path ray and the indirect path ray at each array element is calculated to determine the array response to the reflected signal. The DOA θ is the angle from the broad side of the array as depicted in figure 4.6. The path length difference is computed based on the geometry of figure 4.6:

$$P_1 + P_2 = 2(P + i \cdot d) \sin \theta, \quad (4.37)$$

where i is the array element number with respect to the phase center of the array as defined in figure 4.6, and d is the array sensor spacing. The path lengths P_1 and P_2 sum to give the total path length difference between the direct and indirect path rays at the i th sensor. With this path length difference at each element, the reflected signal can be represented as

$$x_2(t, i) = \rho_r x_1 \left(t - \frac{2(P + i \cdot d) \sin \theta}{c}, i \right), \quad (4.38)$$

where c is the propagation speed. The total signal can be represented as the sum of two signals, the direct path signal and the reflected one as follows:

$$\mathbf{s} = \mathbf{s}_1 + \mathbf{s}_2. \quad (4.39)$$

The data covariance matrix can now be computed as

$$\begin{aligned} R_{\mathbf{x}} &= E[\mathbf{s}\mathbf{s}^H] + R_{nn} \\ &= E[(\mathbf{s}_1 + \mathbf{s}_2)(\mathbf{s}_1^H + \mathbf{s}_2^H)] + R_{nn} \\ &= E[\mathbf{s}_1\mathbf{s}_1^H] + E[\mathbf{s}_1\mathbf{s}_2^H] + E[\mathbf{s}_2\mathbf{s}_1^H] + E[\mathbf{s}_2\mathbf{s}_2^H] + R_{nn} \\ &= R_{\mathbf{s}_1} + R_{\mathbf{s}_1\mathbf{s}_2} + R_{\mathbf{s}_2\mathbf{s}_1} + R_{\mathbf{s}_2} + R_{nn}, \end{aligned} \quad (4.40)$$

where

$$\begin{aligned} R_{\mathbf{s}_1} &= \int_{\Omega} S(\omega) \mathbf{d}_1(\omega, \theta) \mathbf{d}_1^H(\omega, \theta) d\omega \\ R_{\mathbf{s}_1\mathbf{s}_2} &= \int_{\Omega} S(\omega) \mathbf{d}_1(\omega, \theta) \mathbf{d}_2^H(\omega, \theta) d\omega \\ R_{\mathbf{s}_2\mathbf{s}_1} &= \int_{\Omega} S(\omega) \mathbf{d}_2(\omega, \theta) \mathbf{d}_1^H(\omega, \theta) d\omega \\ R_{\mathbf{s}_2} &= \int_{\Omega} S(\omega) \mathbf{d}_2(\omega, \theta) \mathbf{d}_2^H(\omega, \theta) d\omega \\ R_{nn} &= \sigma_n^2 I, \end{aligned} \quad (4.41)$$

with \mathbf{d}_1 the array response vector of the direct path signal as originally defined, \mathbf{d}_2 the array response vector of the reflected signal modified according to equation 4.38, and σ_n^2 the noise power.

The array response vectors are expressed as

$$\mathbf{d}_1 = \Psi(e^{-j\omega T}) \otimes \begin{bmatrix} \vdots \\ e^{j1\omega \frac{L}{c} \sin \theta} \\ 1 \\ e^{-j1\omega \frac{L}{c} \sin \theta} \\ \vdots \end{bmatrix}$$

and

$$\begin{aligned} \mathbf{d}_2 &= \Psi(e^{-j\omega T}) \otimes \rho_r \begin{bmatrix} \vdots \\ e^{j1\omega \frac{L}{c} \sin \theta} e^{-j\omega 2 \frac{(P+d)}{c} \sin \theta} \\ 1 \cdot e^{-j\omega 2 \frac{P}{c} \sin \theta} \\ e^{-j1\omega \frac{L}{c} \sin \theta} e^{-j\omega 2 \frac{(P-d)}{c} \sin \theta} \\ \vdots \end{bmatrix} \\ &= \Psi(e^{-j\omega T}) \otimes \rho_r \begin{bmatrix} \vdots \\ e^{j1\omega \frac{L}{c} \sin \theta} e^{-j\omega 2 \frac{P}{c} \sin \theta} e^{-j\omega 2 \frac{d}{c} \sin \theta} \\ 1 \cdot e^{-j\omega 2 \frac{P}{c} \sin \theta} \\ e^{-j1\omega \frac{L}{c} \sin \theta} e^{-j\omega 2 \frac{P}{c} \sin \theta} e^{j\omega 2 \frac{d}{c} \sin \theta} \\ \vdots \end{bmatrix} \\ &= \Psi(e^{-j\omega T}) \otimes \rho_r e^{-j\omega 2 \frac{P}{c} \sin \theta} \begin{bmatrix} \vdots \\ e^{-j1\omega \frac{L}{c} \sin \theta} \\ 1 \\ e^{j1\omega \frac{L}{c} \sin \theta} \\ \vdots \end{bmatrix}. \end{aligned} \quad (4.42)$$

The last equation can be written as

$$\mathbf{d}_2 = \rho_r e^{-j\omega 2 \frac{P}{c} \sin \theta} \mathbf{d}_1(\omega, -\theta). \quad (4.43)$$

The above equations for the array response vectors indicate that the direct path signal covariance matrix is the same as previously defined. The covariance matrix of the second (reflected) signal is just ρ_r^2 times the previously defined signal covariance matrix computed for the negative of the angle of the first signal. The expressions for the cross term signal covariance matrices are new and must be determined. Substituting the PSD and second array response vector in 4.41 leads to

$$\begin{aligned} R_{s_1 s_2} &= \frac{1}{4\pi} \rho_r \int_{-\omega_b}^{-\omega_a} e^{j\omega 2 \frac{P}{c} \sin \theta} \mathbf{d}_1(\omega, \theta) \mathbf{d}_1^H(\omega, -\theta) d\omega + \frac{1}{4\pi} \rho_r \int_{\omega_a}^{\omega_b} e^{j\omega 2 \frac{P}{c} \sin \theta} \mathbf{d}_1(\omega, \theta) \mathbf{d}_1^H(\omega, -\theta) d\omega \\ &= \frac{1}{4\pi} \rho_r \int_{-\omega_b}^{-\omega_a} e^{j\omega 2 \frac{P}{c} \sin \theta} [e^{j\omega \frac{K-1}{2} \frac{d}{c} \sin \theta} \mathbf{\Phi}_L \otimes \mathbf{\Phi}_K] [e^{-j\omega \frac{K-1}{2} \frac{d}{c} \sin \theta} \mathbf{\Phi}_L \otimes \mathbf{\Phi}_K^*]^H d\omega \\ &\quad + \frac{1}{4\pi} \rho_r \int_{\omega_a}^{\omega_b} e^{j\omega 2 \frac{P}{c} \sin \theta} [e^{j\omega \frac{K-1}{2} \frac{d}{c} \sin \theta} \mathbf{\Phi}_L \otimes \mathbf{\Phi}_K] [e^{-j\omega \frac{K-1}{2} \frac{d}{c} \sin \theta} \mathbf{\Phi}_L \otimes \mathbf{\Phi}_K^*]^H d\omega \\ &= \frac{1}{4\pi} \rho_r \int_{-\omega_b}^{-\omega_a} e^{j\omega 2 \frac{P}{c} \sin \theta} [e^{j\omega \frac{K-1}{2} \frac{d}{c} \sin \theta} \mathbf{\Phi}_L \otimes \mathbf{\Phi}_K] [e^{j\omega \frac{K-1}{2} \frac{d}{c} \sin \theta} \mathbf{\Phi}_L^H \otimes \mathbf{\Phi}_K^{*H}] d\omega \\ &\quad + \frac{1}{4\pi} \rho_r \int_{\omega_a}^{\omega_b} e^{j\omega 2 \frac{P}{c} \sin \theta} [e^{j\omega \frac{K-1}{2} \frac{d}{c} \sin \theta} \mathbf{\Phi}_L \otimes \mathbf{\Phi}_K] [e^{j\omega \frac{K-1}{2} \frac{d}{c} \sin \theta} \mathbf{\Phi}_L^H \otimes \mathbf{\Phi}_K^{*H}] d\omega \\ &= \frac{1}{4\pi} \rho_r \int_{-\omega_b}^{-\omega_a} e^{j\omega 2 \frac{P}{c} \sin \theta} e^{j\omega(K-1) \frac{d}{c} \sin \theta} [\mathbf{\Phi}_L \mathbf{\Phi}_L^H] \otimes [\mathbf{\Phi}_K \mathbf{\Phi}_K^T] d\omega \\ &\quad + \frac{1}{4\pi} \rho_r \int_{\omega_a}^{\omega_b} e^{j\omega 2 \frac{P}{c} \sin \theta} e^{j\omega(K-1) \frac{d}{c} \sin \theta} [\mathbf{\Phi}_L \mathbf{\Phi}_L^H] \otimes [\mathbf{\Phi}_K \mathbf{\Phi}_K^T] d\omega, \end{aligned} \quad (4.44)$$

where $\mathbf{\Phi}_L \mathbf{\Phi}_L^H$ is defined in equation 4.21. Again, the arguments of $\mathbf{\Phi}_L$ and $\mathbf{\Phi}_K$ have been dropped and are $e^{-j\omega T}$ and $e^{-j\omega \frac{d}{c} \sin \theta}$, respectively. Define $D(\omega, \theta)$ as

$$D(\omega, \theta) = e^{j\omega(K-1) \frac{d}{c} \sin \theta} \mathbf{\Phi}_K \mathbf{\Phi}_K^T = \begin{bmatrix} e^{j(K-1)\omega \frac{d}{c} \sin \theta} & e^{j(K-2)\omega \frac{d}{c} \sin \theta} & \dots & 1 \\ e^{j(K-2)\omega \frac{d}{c} \sin \theta} & e^{j(K-3)\omega \frac{d}{c} \sin \theta} & \dots & e^{-j1\omega \frac{d}{c} \sin \theta} \\ \vdots & \vdots & \vdots & \vdots \\ 1 & e^{-j1\omega \frac{d}{c} \sin \theta} & \dots & e^{-j(K-1)\omega \frac{d}{c} \sin \theta} \end{bmatrix}. \quad (4.45)$$

The cross covariance matrix can then be written compactly as

$$R_{s_1 s_2} = \frac{1}{4\pi} \rho_r \int_{-\omega_b}^{-\omega_a} e^{j\omega 2 \frac{P}{c} \sin \theta} \cdot A(\omega) \otimes D(\omega, \theta) d\omega + \frac{1}{4\pi} \rho_r \int_{\omega_a}^{\omega_b} e^{j\omega 2 \frac{P}{c} \sin \theta} \cdot A(\omega) \otimes D(\omega, \theta) d\omega. \quad (4.46)$$

$R_{s_1 s_2}$ can now be written as

$$\begin{aligned} & \frac{1}{4\pi} \rho_r \begin{bmatrix} \int_{-\omega_b}^{-\omega_a} e^{j\omega 2 \frac{P}{c} \sin \theta} a_0 D d\omega & \int_{-\omega_b}^{-\omega_a} e^{j\omega 2 \frac{P}{c} \sin \theta} a_1 D d\omega & \dots & \int_{-\omega_b}^{-\omega_a} e^{j\omega 2 \frac{P}{c} \sin \theta} a_{(L-1)} D d\omega \\ \int_{-\omega_b}^{-\omega_a} e^{j\omega 2 \frac{P}{c} \sin \theta} a_{-1} D d\omega & \int_{-\omega_b}^{-\omega_a} e^{j\omega 2 \frac{P}{c} \sin \theta} a_0 D d\omega & \dots & \int_{-\omega_b}^{-\omega_a} e^{j\omega 2 \frac{P}{c} \sin \theta} a_{(L-2)} D d\omega \\ \vdots & \vdots & \vdots & \vdots \\ \int_{-\omega_b}^{-\omega_a} e^{j\omega 2 \frac{P}{c} \sin \theta} a_{-(L-1)} D d\omega & \dots & \dots & \int_{-\omega_b}^{-\omega_a} e^{j\omega 2 \frac{P}{c} \sin \theta} a_0 D d\omega \end{bmatrix} \\ & + \frac{1}{4\pi} \rho_r \begin{bmatrix} \int_{\omega_a}^{\omega_b} e^{j\omega 2 \frac{P}{c} \sin \theta} a_0 D d\omega & \int_{\omega_a}^{\omega_b} e^{j\omega 2 \frac{P}{c} \sin \theta} a_1 D d\omega & \dots & \int_{\omega_a}^{\omega_b} e^{j\omega 2 \frac{P}{c} \sin \theta} a_{(L-1)} D d\omega \\ \int_{\omega_a}^{\omega_b} e^{j\omega 2 \frac{P}{c} \sin \theta} a_{-1} D d\omega & \int_{\omega_a}^{\omega_b} e^{j\omega 2 \frac{P}{c} \sin \theta} a_0 D d\omega & \dots & \int_{\omega_a}^{\omega_b} e^{j\omega 2 \frac{P}{c} \sin \theta} a_{(L-2)} D d\omega \\ \vdots & \vdots & \vdots & \vdots \\ \int_{\omega_a}^{\omega_b} e^{j\omega 2 \frac{P}{c} \sin \theta} a_{-(L-1)} D d\omega & \dots & \dots & \int_{\omega_a}^{\omega_b} e^{j\omega 2 \frac{P}{c} \sin \theta} a_0 D d\omega \end{bmatrix}, \end{aligned} \quad (4.47)$$

where $a_{i_1} = e^{j i_1 \omega T}$ and the arguments of D have been dropped. The above matrix is block Toeplitz.

The whole matrix can be formed by calculating the blocks of the first row and column and creating a Toeplitz matrix. This is done using Matlab. The block on the i_1^{th} principal diagonal of the above matrix is a Hankel matrix of the form

$$R(i_1) = \int_{-\omega_b}^{-\omega_a} e^{j\omega 2 \frac{P}{c} \sin \theta} e^{j i_1 \omega T} D(\omega, \theta) d\omega + \int_{\omega_a}^{\omega_b} e^{j\omega 2 \frac{P}{c} \sin \theta} e^{j i_1 \omega T} D(\omega, \theta) d\omega. \quad (4.48)$$

The elements on the i_2^{th} minor diagonal of $R(i_1)$ are

$$r(i_1, i_2) = \int_{-\omega_b}^{-\omega_a} e^{j\omega 2 \frac{P}{c} \sin \theta} e^{j i_1 \omega T} e^{j i_2 \omega \frac{L}{c} \sin \theta} d\omega + \int_{\omega_a}^{\omega_b} e^{j\omega 2 \frac{P}{c} \sin \theta} e^{j i_1 \omega T} e^{j i_2 \omega \frac{L}{c} \sin \theta} d\omega. \quad (4.49)$$

The variable i_1 ranges from $-(L-1)$ to $(L-1)$ in increments of 1. The variable i_2 ranges from $-(K-1)$ to $(K-1)$ in increments of 1. Each element of the signal covariance matrix is of the following form:

$$\begin{aligned}
 r(i_1, i_2) &= \frac{1}{4\pi} \rho_r \int_{-\omega_b}^{-\omega_a} e^{j\omega[i_1 T + 2\frac{P}{c} \sin \theta + i_2 \frac{d}{c} \sin \theta]} d\omega + \frac{1}{4\pi} \rho_r \int_{\omega_a}^{\omega_b} e^{j\omega[i_1 T + 2\frac{P}{c} \sin \theta + i_2 \frac{d}{c} \sin \theta]} d\omega \\
 &= \rho_r \frac{e^{-j\omega_a[i_1 T + 2\frac{P}{c} \sin \theta + i_2 \frac{d}{c} \sin \theta]} - e^{-j\omega_b[i_1 T + 2\frac{P}{c} \sin \theta + i_2 \frac{d}{c} \sin \theta]}}{4\pi j[i_1 T + 2\frac{P}{c} \sin \theta + i_2 \frac{d}{c} \sin \theta]} \\
 &\quad + \rho_r \frac{e^{j\omega_b[i_1 T + 2\frac{P}{c} \sin \theta + i_2 \frac{d}{c} \sin \theta]} - e^{j\omega_a[i_1 T + 2\frac{P}{c} \sin \theta + i_2 \frac{d}{c} \sin \theta]}}{4\pi j[i_1 T + 2\frac{P}{c} \sin \theta + i_2 \frac{d}{c} \sin \theta]} \\
 &= \rho_r \frac{\sin[\omega_b T(i_1 T + 2\frac{P}{c} \sin \theta + i_2 \frac{d}{c} \sin \theta)]}{2\pi(i_1 T + 2\frac{P}{c} \sin \theta + i_2 \frac{d}{c} \sin \theta)} \\
 &\quad - \rho_r \frac{\sin[\omega_a T(i_1 T + 2\frac{P}{c} \sin \theta + i_2 \frac{d}{c} \sin \theta)]}{2\pi(i_1 T + 2\frac{P}{c} \sin \theta + i_2 \frac{d}{c} \sin \theta)} \\
 &= \rho_r \frac{\omega_b T \cdot \text{sinc}[\omega_b(i_1 T + 2\frac{P}{c} \sin \theta + i_2 \frac{d}{c} \sin \theta)]}{2\pi} \\
 &\quad - \rho_r \frac{\omega_a T \cdot \text{sinc}[\omega_a(i_1 T + 2\frac{P}{c} \sin \theta + i_2 \frac{d}{c} \sin \theta)]}{2\pi}. \tag{4.50}
 \end{aligned}$$

The file `mscm12h.m` computes this cross signal covariance matrix. The other cross covariance matrix, $R_{s_2 s_1}$, is calculated in the same manner. The structure of $R_{s_2 s_1}$ is the same as $R_{s_1 s_2}$. Its elements can be expressed as

$$\begin{aligned}
 r(i_1, i_2) &= \rho_r \frac{\omega_b T \cdot \text{sinc}[\omega_b(i_1 T - 2\frac{P}{c} \sin \theta + i_2 \frac{d}{c} \sin \theta)]}{2\pi} \\
 &\quad - \rho_r \frac{\omega_a T \cdot \text{sinc}[\omega_a(i_1 T - 2\frac{P}{c} \sin \theta + i_2 \frac{d}{c} \sin \theta)]}{2\pi}. \tag{4.51}
 \end{aligned}$$

The file `mscm21h.m` computes this cross signal covariance matrix.

4.3.2 Eigenvector Constraints.

4.3.2.1 General Case. The broadband constraint

$$\mathbf{w}^H \mathbf{d}(\omega, \theta) = r(\omega, \theta) \quad \text{for } \omega_a \leq \omega \leq \omega_b, \theta_a \leq \theta \leq \theta_b \quad (4.52)$$

consists of an infinite number of constraints as opposed to a point constraint in the narrowband case. Writing many constraints at specified frequencies and angles would be inefficient because each constraint uses up one degree of freedom. Also, the constraints would hold at only the specified frequency and angle pairs. There would be no control over the response at frequency and angle pairs other than the specified ones. For this reason, Van Veen [40] defines eigenvector constraints which minimize the total squared error between the desired response and the actual response over the entire frequency and angle extent while using up a fixed number of degrees of freedom. Defining r_d as the desired response, the total squared error between the desired and actual response is

$$e^2 = \frac{1}{4\pi} \int_{-\theta_b}^{-\theta_a} \int_{-\omega_b}^{-\omega_a} |r_d(\theta, \omega) - \mathbf{w}^H \mathbf{d}(\theta, \omega)|^2 d\omega d\theta + \frac{1}{4\pi} \int_{\theta_a}^{\theta_b} \int_{\omega_a}^{\omega_b} |r_d(\theta, \omega) - \mathbf{w}^H \mathbf{d}(\theta, \omega)|^2 d\omega d\theta. \quad (4.53)$$

The problem is to minimize this total squared error subject to keeping a fixed number of constraints.

The factor $\frac{1}{4\pi}$ is included for convenience. With the previous definition of R_s ,

$$R_s = \frac{1}{4\pi} \int_{-\theta_b}^{-\theta_a} \int_{-\omega_b}^{-\omega_a} \mathbf{d}(\theta, \omega) \mathbf{d}^H(\theta, \omega) d\omega d\theta + \frac{1}{4\pi} \int_{\theta_a}^{\theta_b} \int_{\omega_a}^{\omega_b} \mathbf{d}(\theta, \omega) \mathbf{d}^H(\theta, \omega) d\omega d\theta,$$

the problem is stated as

$$\begin{aligned} \min_{\mathbf{w}} & \left[\mathbf{w}^T R_s \mathbf{w} - \frac{1}{4\pi} \mathbf{w}^T \int_{-\theta_b}^{-\theta_a} \int_{-\omega_b}^{-\omega_a} r_d^*(\theta, \omega) \mathbf{d}(\theta, \omega) d\omega d\theta \right. \\ & \left. - \frac{1}{4\pi} \left(\int_{-\theta_b}^{-\theta_a} \int_{-\omega_b}^{-\omega_a} r_d(\theta, \omega) \mathbf{d}^{*T}(\theta, \omega) d\omega d\theta \right) \mathbf{w} \right] \end{aligned}$$

$$- \frac{1}{4\pi} \mathbf{w}^T \int_{\theta_a}^{\theta_b} \int_{\omega_a}^{\omega_b} r_d^*(\theta, \omega) \mathbf{d}(\theta, \omega) d\omega d\theta - \frac{1}{4\pi} \left(\int_{\theta_a}^{\theta_b} \int_{\omega_a}^{\omega_b} r_d(\theta, \omega) \mathbf{d}^*(\theta, \omega) d\omega d\theta \right) \mathbf{w}], \quad (4.54)$$

where the transpose operator is substituted for the Hermitian since the data and weights are real and the terms excluding \mathbf{w} are eliminated. After taking the gradient with respect to \mathbf{w} and setting the equation equal to zero, this can be arranged as

$$\begin{aligned} R_s \mathbf{w} = & \frac{1}{8\pi} \int_{\theta_a}^{\theta_b} \int_{\omega_a}^{\omega_b} r_d^*(-\theta, -\omega) \mathbf{d}(-\theta, -\omega) d\omega d\theta \\ & + \frac{1}{8\pi} \int_{\theta_a}^{\theta_b} \int_{\omega_a}^{\omega_b} r_d(-\theta, -\omega) \mathbf{d}^*(-\theta, -\omega) d\omega d\theta \\ & + \frac{1}{8\pi} \int_{\theta_a}^{\theta_b} \int_{\omega_a}^{\omega_b} r_d^*(\theta, \omega) \mathbf{d}(\theta, \omega) d\omega d\theta + \frac{1}{8\pi} \int_{\theta_a}^{\theta_b} \int_{\omega_a}^{\omega_b} r_d(\theta, \omega) \mathbf{d}^*(\theta, \omega) d\omega d\theta. \end{aligned} \quad (4.55)$$

Define \mathbf{f} as follows:

$$\begin{aligned} \mathbf{f} = & \frac{1}{8\pi} \int_{\theta_a}^{\theta_b} \int_{\omega_a}^{\omega_b} r_d^*(-\theta, -\omega) \mathbf{d}(-\theta, -\omega) d\omega d\theta + \frac{1}{8\pi} \int_{\theta_a}^{\theta_b} \int_{\omega_a}^{\omega_b} r_d(-\theta, -\omega) \mathbf{d}^*(-\theta, -\omega) d\omega d\theta \\ & + \frac{1}{8\pi} \int_{\theta_a}^{\theta_b} \int_{\omega_a}^{\omega_b} r_d^*(\theta, \omega) \mathbf{d}(\theta, \omega) d\omega d\theta + \frac{1}{8\pi} \int_{\theta_a}^{\theta_b} \int_{\omega_a}^{\omega_b} r_d(\theta, \omega) \mathbf{d}^*(\theta, \omega) d\omega d\theta. \end{aligned} \quad (4.56)$$

By properly choosing the desired response, equation 4.56 can be solved. Constrain the response to have unit gain and linear phase with the response defined as

$$r_d = e^{-j(\frac{L-1}{2})\omega T} \quad (4.57)$$

This amount of delay is required for a natural beamformer response. If you do not allow enough delay in the constrained response, the beamformer will not have time for weighting and summing enough of the delayed data at the sensors and taps to meet the constraint.

Each of the four integrals is solved separately to obtain f . The first integral is solved by

$$\begin{aligned}
 & \int_{\theta_a}^{\theta_b} \int_{\omega_a}^{\omega_b} r_d^*(-\theta, -\omega) d(-\theta, -\omega) d\omega \\
 &= \iint e^{-j(\frac{L-1}{2})\omega T} \begin{bmatrix} 1 \\ e^{j(1)\omega T} \\ \vdots \\ e^{j(L-1)\omega T} \end{bmatrix} \otimes \begin{bmatrix} e^{j\omega(\frac{K-1}{2})\frac{4}{c} \sin \theta} \\ e^{j\omega(\frac{K-1}{2}-1)\frac{4}{c} \sin \theta} \\ \vdots \\ e^{j\omega(\frac{K-1}{2}-K+1)\frac{4}{c} \sin \theta} \end{bmatrix} d\omega d\theta \\
 &= \iint \begin{bmatrix} e^{-j(\frac{L-1}{2})\omega T} \\ e^{-j(\frac{L-1}{2}-1)\omega T} \\ \vdots \\ e^{-j(\frac{L-1}{2}-L+1)\omega T} \end{bmatrix} \otimes \begin{bmatrix} e^{j\omega(\frac{K-1}{2})\frac{4}{c} \sin \theta} \\ e^{j\omega(\frac{K-1}{2}-1)\frac{4}{c} \sin \theta} \\ \vdots \\ e^{j\omega(\frac{K-1}{2}-K+1)\frac{4}{c} \sin \theta} \end{bmatrix} d\omega d\theta. \quad (4.58)
 \end{aligned}$$

Each of the elements in the above vector can now be expressed as

$$\gamma(i_1) = \iint e^{-ji_1\omega T} \begin{bmatrix} e^{j\omega(\frac{K-1}{2})\frac{4}{c} \sin \theta} \\ e^{j\omega(\frac{K-1}{2}-1)\frac{4}{c} \sin \theta} \\ \vdots \\ e^{j\omega(\frac{K-1}{2}-K+1)\frac{4}{c} \sin \theta} \end{bmatrix} d\omega d\theta = \begin{bmatrix} \gamma(\frac{K-1}{2}) \\ \gamma(\frac{K-1}{2}-1) \\ \vdots \\ \gamma(\frac{K-1}{2}-K+1) \end{bmatrix}, \quad (4.59)$$

where each of the γ_{-i_2} s is of the form

$$\gamma_{-i_2} = \iint e^{-ji_1\omega T} e^{-ji_2\omega \frac{4}{c} \sin \theta} d\omega d\theta \quad (4.60)$$

with i_1 fixed. The variable i_1 ranges from $\frac{L-1}{2}$ to $\frac{L-1}{2} - L + 1$. The variable i_2 ranges from $\frac{-K+1}{2}$ to $\frac{-K+1}{2} + K - 1$. The other integrals can be solved in a similar manner to the first one. The resulting equations and ranges of indices are provided below. The elements of the second integral

in equation 4.56 are of the form

$$\gamma_{i_2} = \int e^{j i_1 \omega T} e^{j i_2 \omega \frac{d}{c} \sin \theta} d\omega \quad (4.61)$$

with i_1 fixed. The variable i_1 ranges from $\frac{L-1}{2}$ to $\frac{L-1}{2} - L + 1$. The variable i_2 ranges from $\frac{-K+1}{2}$ to $\frac{-K+1}{2} + K - 1$. The elements of the third integral in equation 4.56 are of the form

$$\gamma_{i_2} = \int e^{j i_1 \omega T} e^{j i_2 \omega \frac{d}{c} \sin \theta} d\omega \quad (4.62)$$

with i_1 fixed. The variable i_1 ranges from $\frac{L-1}{2}$ to $\frac{L-1}{2} - L + 1$. The variable i_2 ranges from $\frac{K-1}{2}$ to $\frac{K-1}{2} - K + 1$. The elements of the fourth integral in equation 4.56 are of the form

$$\gamma_{-i_2} = \int e^{-j i_1 \omega T} e^{-j i_2 \omega \frac{d}{c} \sin \theta} d\omega \quad (4.63)$$

with i_1 fixed. The variable i_1 ranges from $\frac{L-1}{2}$ to $\frac{L-1}{2} - L + 1$. The variable i_2 ranges from $\frac{K-1}{2}$ to $\frac{K-1}{2} - K + 1$.

Since I had already written the following algorithm, the first plus second integrals were computed and the third plus the fourth to find the elements of f:

$$\begin{aligned} f(i_1, i_2) &= \frac{1}{8\pi} \int_{\theta_a}^{\theta_b} \left(\int_{\omega_a}^{\omega_b} e^{j\omega[i_1 T + i_2 \frac{d}{c} \sin \theta]} d\omega \right) d\theta + \frac{1}{8\pi} \int_{\theta_a}^{\theta_b} \left(\int_{\omega_a}^{\omega_b} e^{-j\omega[i_1 T + i_2 \frac{d}{c} \sin \theta]} d\omega \right) d\theta \\ &= \frac{1}{8\pi} \int_{\theta_a}^{\theta_b} \frac{e^{j\omega_b[i_1 T + i_2 \frac{d}{c} \sin \theta]} - e^{j\omega_a[i_1 T + i_2 \frac{d}{c} \sin \theta]}}{j[i_1 T + i_2 \frac{d}{c} \sin \theta]} d\theta + \frac{1}{8\pi} \int_{\theta_a}^{\theta_b} \frac{e^{-j\omega_b[i_1 T + i_2 \frac{d}{c} \sin \theta]} - e^{-j\omega_a[i_1 T + i_2 \frac{d}{c} \sin \theta]}}{-j[i_1 T + i_2 \frac{d}{c} \sin \theta]} d\theta \\ &= \frac{1}{8\pi} \int_{\theta_a}^{\theta_b} \frac{e^{j\omega_b[i_1 T + i_2 \frac{d}{c} \sin \theta]} - e^{j\omega_a[i_1 T + i_2 \frac{d}{c} \sin \theta]}}{j[i_1 T + i_2 \frac{d}{c} \sin \theta]} + \frac{e^{-j\omega_b[i_1 T + i_2 \frac{d}{c} \sin \theta]} - e^{-j\omega_a[i_1 T + i_2 \frac{d}{c} \sin \theta]}}{-j[i_1 T + i_2 \frac{d}{c} \sin \theta]} d\theta \\ &\approx \frac{1}{8\pi} \sum_{j=1}^J \frac{e^{j\omega_b[i_1 T + i_2 \frac{d}{c} \sin \theta]} - e^{j\omega_a[i_1 T + i_2 \frac{d}{c} \sin \theta]}}{j[i_1 T + i_2 \frac{d}{c} \sin \theta]} + \frac{e^{-j\omega_b[i_1 T + i_2 \frac{d}{c} \sin \theta]} - e^{-j\omega_a[i_1 T + i_2 \frac{d}{c} \sin \theta]}}{-j[i_1 T + i_2 \frac{d}{c} \sin \theta]} \Delta\theta. \end{aligned} \quad (4.64)$$

The above equation can be used to compute the first pair and the second pair of integrals since the pairs have common ranges for the indices of i_1 and i_2 . Each of the pairs of integrals is of the form

$$f(i_1, i_2) = \frac{1}{8\pi} \int_{\theta_a}^{\theta_b} \int_{\omega_a}^{\omega_b} e^{j\omega[i_1 T + i_2 \frac{d}{c} \sin \theta]} d\omega d\theta + \frac{1}{8\pi} \int_{\theta_a}^{\theta_b} \int_{\omega_a}^{\omega_b} e^{-j\omega[i_1 T + i_2 \frac{d}{c} \sin \theta]} d\omega d\theta. \quad (4.65)$$

The files `ftdb.m` and `fdb.m` implement the above integrals with a Riemann sum. Equation 4.55 can be written in vector notation as

$$R_s \mathbf{w} = \mathbf{f}. \quad (4.66)$$

This is in the same form as the linear constraints previously defined as

$$C^H \mathbf{w} = \mathbf{g}, \quad (4.67)$$

with R_s in the place of the Hermitian of the constraint matrix and \mathbf{f} in place of \mathbf{g} . Performing a low rank approximation on R_s will be more efficient by using less degrees of freedom than all of the columns of R_s . Keeping most of the energy of the eigenvalues provides a good approximation to higher rank matrix, R_s . The signal covariance matrix can be written

$$R_s \approx U \Sigma_r V^H, \quad (4.68)$$

where Σ_r is a diagonal matrix containing all or most of the nonzero eigenvalues. Based on Buckley's [5] time bandwidth product for sources at a single angle, a formula is developed which provides good results for the multiple angle case. The number of constraints, D , used in the low rank approximation is computed as

$$D = \lceil [(K-1) \left\{ \frac{d}{c} \sin \theta_2 - \frac{d}{c} \sin \theta_1 \right\} + (L-1)T] 2(f_2 - f_1) + 1 \rceil, \quad (4.69)$$

where $\lceil x \rceil$ is defined as the integer greater than or equal to x . Substituting equation 4.68 in equation 4.66 and noting that U is a unitary matrix ($U^H U = I$) yields

$$\begin{aligned}
 U \Sigma_r V^H \mathbf{w} &= \mathbf{f} \\
 U^H U \Sigma_r V^H \mathbf{w} &= U^H \mathbf{f} \\
 \Sigma_r^{-1} \Sigma_r V^H \mathbf{w} &= \Sigma_r^{-1} U^H \mathbf{f} \\
 V^H \mathbf{w} &= \Sigma_r^{-1} U^H \mathbf{f} \\
 V^H \mathbf{w} &= \mathbf{f}'.
 \end{aligned} \tag{4.70}$$

This in again in the form of the constraint equation

$$C^H \mathbf{w} = \mathbf{g}, \tag{4.71}$$

with $C = V$ and $\mathbf{g} = \mathbf{f}' = \Sigma_r^{-1} U^H \mathbf{f}$. These values can be substituted in the optimum weight equation to determine the steady state weights.

When the angle of the source is a fixed point, θ_o , \mathbf{f} is defined as

$$\begin{aligned}
 \mathbf{f} &= \frac{1}{8\pi} \int_{\omega_a}^{\omega_b} r_d^*(\theta_o, -\omega) d(\theta_o, -\omega) d\omega + \frac{1}{8\pi} \int_{\omega_a}^{\omega_b} r_d(\theta_o, -\omega) d^*(\theta_o, -\omega) d\omega \\
 &+ \frac{1}{8\pi} \int_{\omega_a}^{\omega_b} r_d^*(\theta_o, \omega) d(\theta_o, \omega) d\omega + \frac{1}{8\pi} \int_{\omega_a}^{\omega_b} r_d(\theta_o, \omega) d^*(\theta_o, \omega) d\omega,
 \end{aligned} \tag{4.72}$$

in equation 4.66. In this case, the number of constraints used, D , is based on capturing 99.99 percent or more of the energy represented by the eigenvalues of R_s . The fraction of energy in the eigenvalues is calculated as

$$f_\lambda = \frac{\sum_{i=1}^D \lambda_i}{\sum_{i=1}^N \lambda_i}, \tag{4.73}$$

where $N = K \times L$. The elements of \mathbf{f} are found as

$$f(i_1, i_2) = \frac{1}{2\pi} \{ \omega_b \text{sinc}[\omega_b(i_1 T + i_2 \frac{d}{c} \sin \theta)] - \omega_a \text{sinc}[\omega_a(i_1 T + i_2 \frac{d}{c} \sin \theta)] \}. \quad (4.74)$$

Equation 4.74 holds for the multipath model for sources having frequency extent with a slight modification. The desired response must be modified to account for the additional delays through the beamformer associated with the reflected (delayed) signal into the array. The beamformer needs time to weight and sum the signals which are delayed relative to the direct path signal, which is the only signal accounted for in the previous definition of r_d . All of the delayed signals need to be combined to form the output of the beamformer. If all of the delayed data at the sensors and taps are not combined, the constraint response cannot be met. The modified response is

$$r_d = e^{-j(\frac{L-1}{2})\omega T} e^{-j\omega \frac{P}{c} \sin \theta}. \quad (4.75)$$

Computing the same four integrals above with the modified response yields

$$\begin{aligned} \mathbf{f}(i_1, i_2) = & \frac{1}{2\pi} \{ \omega_b \text{sinc}[\omega_b(i_1 T + \frac{P}{c} \cdot \sin \theta + i_2 \frac{d}{c} \sin \theta)] \\ & - \omega_a \text{sinc}[\omega_a(i_1 T + \frac{P}{c} \cdot \sin \theta + i_2 \frac{d}{c} \sin \theta)] \}. \end{aligned} \quad (4.76)$$

The file myfcenref.m implements the eigenvector constraints for the multipath case.

4.3.2.2 Correlated Sources/Multipath Environment. The correlated and multipath signal environments are described next. The signals of the first case are perfectly correlated ($\rho_c = 1$). This example was performed to evaluate the cancellation performance for two correlated undesired signals when one of them arrives in the direction of the main beam. The two undesired signals are assumed to be uncorrelated with the desired signal. The file `bfbbreftn.m` contains the code for this problem. The array has 16 elements equally spaced along a line at one-half the wavelength of the highest frequency employed, π . The tap spacing is normalized to one second. This again normalizes frequency on the interval $-\pi$ to π radians. Twelve eigenvector constraints are employed to ensure unit gain and linear phase over the frequency interval $[2\pi/5, 4\pi/5]$ at negative 45 degrees (main beam). The undesired signals are located at positive 45 degrees (right of array broad side) and negative 45 degrees (left of broad side) with power levels of 20 db relative to the white noise power level. Figure 4.7 shows that a beam is formed in the direction of the signal at +45 degrees

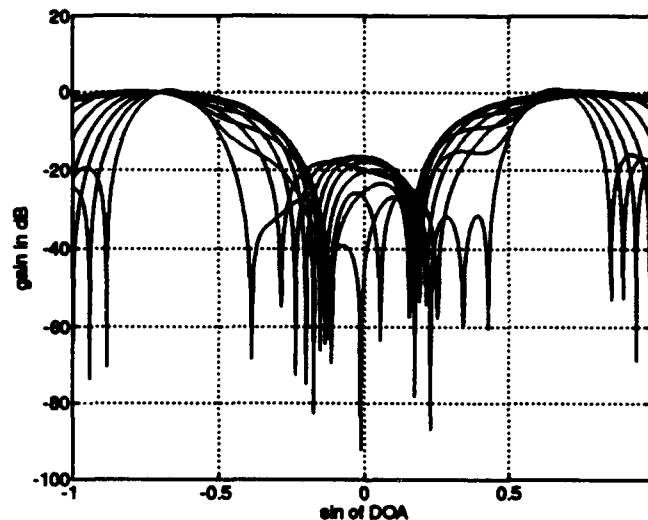


Figure 4.7 Gain of beamformer with correlated signals as a function of DOA for constraint over frequency interval $[2\pi/5, 4\pi/5]$ at -45 degrees plotted at nine frequencies

with the same amplitude level as the signal at -45 degrees. The beamformer's weights adapt to minimize the output power. When the two undesired signals are perfectly correlated, a null is not

formed. The signals are cancelled by destructive addition. In this example, the responses to the two undesired signals are formed so they will cancel (approximately the same amplitude but close to 180 degrees out of phase). The cancellation is computed using the following equation for the beamformer output power:

$$P_o = \mathbf{w}^H \mathbf{R}_{xx} \mathbf{w}. \quad (4.77)$$

The output power for this case is -43.19 dB, which shows that the signals have cancelled well. This cancellation eliminates most of the undesired signal energy at the beamformer output. In the case of a radar in the presence of two correlated jammers (each uncorrelated with the desired signal), this cancellation effect degrades the effectiveness of the jamming. If the signals happen to be correlated desired signals (as can occur with near field multipath scattering into the array), the desired signal will cancel. This is highly undesirable.

The last example is for the case of the radome simulation. A signal arrives from +45 degrees and bounces off a flat plat and into the array at -45 degrees. The direct path signal is assumed to be unaffected by the radome. The metal plate attenuates the signal but is assumed to impart no random phase to the signal. The reflected signal is a scaled and delayed replica of the direct path signal. This simulates a signal bouncing into the main beam. The file bfbfbrefnn.m contains the code for this problem. The array has 16 elements with 25 taps per element. The SNR is 20 dB. The reflected signal is attenuated by one fourth after reflecting from the plate. Ten eigenvector constraints are employed to ensure unit gain and linear phase over the frequency interval $[3\pi/5, 4\pi/5]$ in the desired signal direction of -45 degrees. Figure 4.8 shows the unity constraint at -45 degrees and the beam formed at +45 degrees at one fourth the power. This plot shows a twelve dB drop because it is a plot of the beamformer response squared. The interference cancellation is demonstrated in figures 4.9 and 4.10. Figure 4.9 is the output power of the beamformer with the quiescent weights while figure 4.10 is the output power with the adapted weights due to the source arriving from +45 degrees in addition to the reflection at -45 degrees. These plots are generated

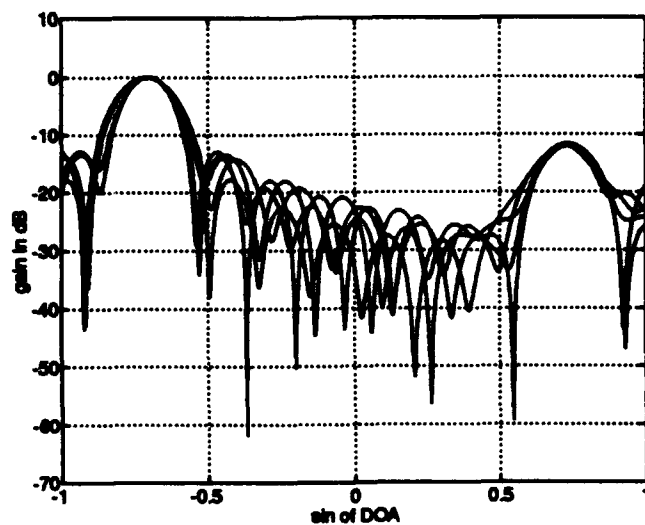


Figure 4.8 Beampattern displaying reflection lobe; SNR = 20 dB

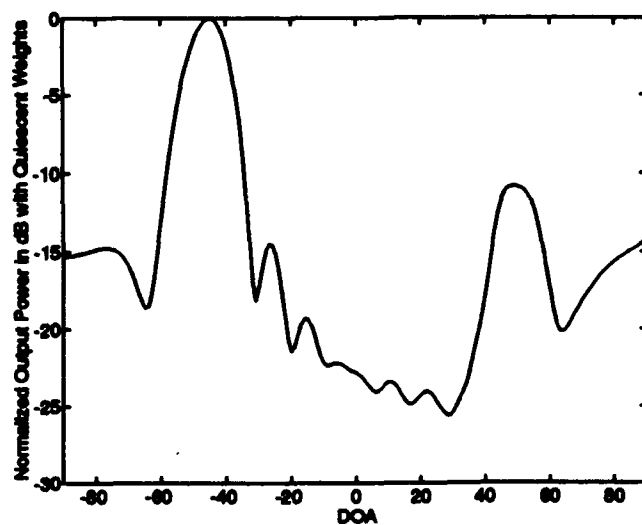


Figure 4.9 Normalized output power with quiescent weights

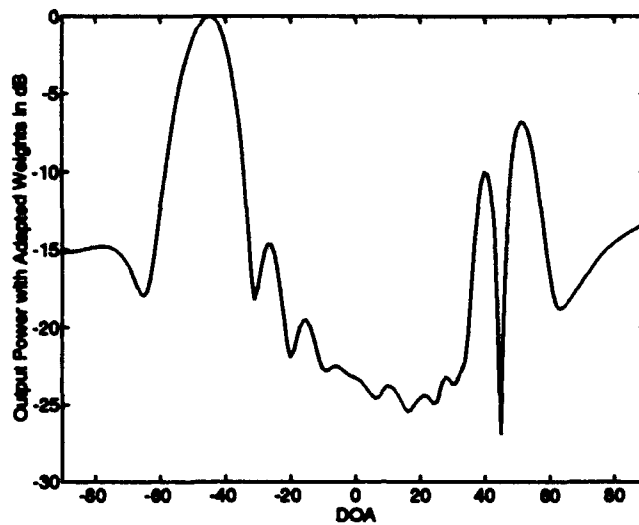


Figure 4.10 Normalized output power with adapted weights

in the same way as the beampatterns. In either case, the weights are first computed for the environment of interest. For the beampattern, the responses due to a narrowband source swept across the directions of arrival are plotted versus DOA. Each of these beampattern plots is for a specific frequency. In the power plots, the output powers due to a broadband source swept across the directions of arrival are plotted. They include the effects of the simulated radome. For this reason, the power plots are like wide band responses. The Matlab files `outputpowq.m` and `outputpoww.m` contain the code to compute and plot the output power. Figure 4.9 can be thought of as installed antenna pattern of a nonadaptive beamformer where the large sidelobes at the negative of the main beam angle are due to RMR. Figure 4.10 can then be thought of as an effective installed antenna pattern of an adaptive beamformer. The actual installed beampattern with adapted weights (figure 4.8) shows that the beamformer actually forms a beam in the interferer direct path direction of +45 degrees. Figure 4.11 is a plot of the beamformer output power as a function of the ratio of the temporal duration of the source to the delay between the direct and indirect path at the phase center. Cancellation is affected by both the temporal duration and the delay. If the delay between the different paths is small enough the correlation can approach unity. The delay was previously

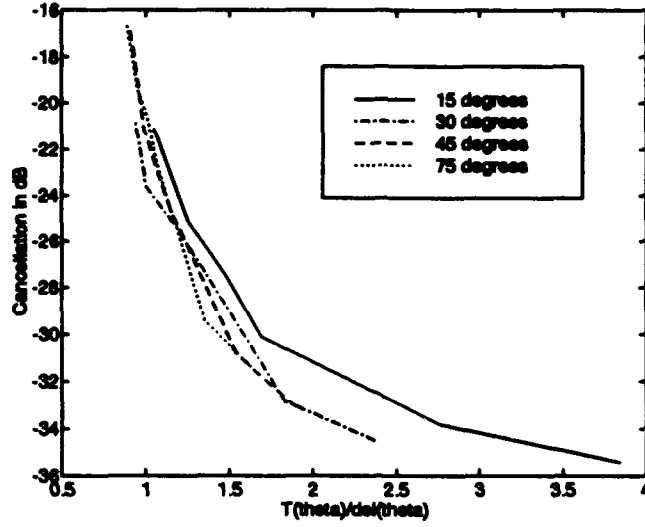


Figure 4.11 Cancellation as a function of the ratio of temporal aperture ($T(\theta)$) to path delay ($del(\theta)$)

defined as

$$del(\theta) = 2P \sin(\theta). \quad (4.78)$$

The delay gets smaller with smaller angles (closer to broadside). Cancellation improves as the correlation increases. For example, the output power with $L = 2$ taps is -16.93 dB at $\theta = 45^\circ$ and -21.15 dB at $\theta = 15^\circ$. For a given angle, the temporal duration increases with increasing number of taps (for a fixed number of sensors). Cancellation performance improves with more taps. For example, at $\theta = 15^\circ$, the output power is -21.15 dB with 2 taps and -35.43 dB with 15 taps.

Another parameter which affects the cancellation performance is the source frequency bandwidth. With the difference in path lengths so small, the major contributor to decorrelation of the signals is the wide bandwidth of the interference signal. The wave field coherence decreases with bandwidth [22]. This is due to the lack of coherence at time differences of

$$\Delta t > \frac{1}{B}, \quad (4.79)$$

where B is the frequency bandwidth. For example, at $\theta = 75^\circ$ with two taps, the output power is -16.7 dB for a source frequency bandwidth of 0.1 and -9.43 dB for a source bandwidth of 0.2.

V. Conclusions and Recommendations

The results obtained show that if the interferer signal reflecting off the radome into the main beam is well correlated with the direct path, the signal can be cancelled without forming a null in the direction of arrival. With the narrowband multipath environment (zero bandwidth), the output power plot shows the cancellation is about 50 dB. With the broadband multipath environment (normalized frequency interval of $[3\pi/5, 4\pi/5]$ radians), the output power plot shows the cancellation is about 20 dB. The cancellation performance improves significantly as the number of taps is increased. For the multipath environment generated in the previous chapter with a $\text{SNR} = 20$ dB, with DOAs of $\pm 20^\circ$ instead of $\pm 45^\circ$, the output power is -21.15 dB with 2 taps and -35.43 dB with 15 taps. As the signal frequency extent increases, the degree of cancellation decreases. For the same multipath environment as noted above with DOAs of $\pm 75^\circ$ and two taps, the output power is -16.7 dB for a source frequency bandwidth of 0.1 and -9.43 dB for a source bandwidth of 0.2. Depending on the frequency bandwidth, a moderate number of taps can be added to obtain good cancellation performance.

Desired signal energy will cancel due to RMR sidelobes in a manner similar to interference signals. In this study, concentration was placed on cancelling reflected interference signals while constraining the beamformer response in the direction of desired signals. The data were generated to consist of interferers. In an actual radome, desired signals may reflect into RMR sidelobes. Since these reflected signals may be correlated with the one in the desired direction (main lobe), part of the desired signal might cancel. The amount of cancellation will be dependent on the actual reflection coefficient of the radome, the bandwidth, and the directions of arrivals of the signals.

The results obtained so far for the GSC are encouraging. The beamformers employed in this thesis are fully adaptive. These beamformers utilize all of the available adaptive degrees of freedom, and are difficult to implement. Each adaptive degree of freedom typically requires a receiver channel. These channels, in addition to the channel needed for the fixed beamformer, are

not easily added to an airborne radar. The next logical step to this thesis is to evaluate interference cancellation performance using only a small number of the adaptive degrees of freedom. This is the subject of partially adaptive beamforming and is discussed in many of the reference articles. Van Veen [40] has written several articles on partially adaptive beamforming.

The method of partially adaptive LCMV beamforming does not require pre-selection of the particular elements which comprise the auxiliary antennas as in the case of the multiple sidelobe canceller. The MSC assumes a known main and auxiliary channel designation. In a GSC, a transformation is performed on the $N - M$ available adaptive degrees of freedom to reduce the number of adaptive weights. A likely interference scenario is developed which contains information such as the maximum number of interferers, their locations and frequency ranges, white noise level, etc.. This information is used to design the transformation matrix, which is built into the array. Since the locations of the jammers are not known, the locations can be guessed to range over the angular field of view of the array (-90° to $+90^\circ$). The beamformer design based on these locations should be evaluated to see how well it works for different test scenarios.

Another area which should be investigated is beampattern control. The normal beampatterns obtained from the LCMV method have typical -13 dB down sidelobes. Most radar applications require much lower sidelobe levels. If a partially adaptive beamformer is designed, the unused adaptive degrees of freedom can be used to approximate a desired quiescent response [20][43]. The quiescent pattern can then be approximated to beampatterns typically obtained by deterministic, nonadaptive arrays.

In this thesis, all frequency is in terms of normalized frequency. Intermediate frequencies (IFs), the IF bandwidth, and the IF sampling rate of a typical X-band radar should be used next.

The radome models can be expanded to include more complex elliptical models which more closely resemble the actual radomes. These models which do not make use of plane waves are very difficult to develop. Actual array data at the individual elements, if available, should be used.

Appendix A. MATLAB Code

All Matlab code used to support this thesis was written by the author.

```
%bf_response.m
clear
n = 20; % number of sensors
lambda = 2; % wavelength
d = 1; % interelement spacing
w = (1/n)*exp(-j*2*pi*d/lambda*.1).^[0:n-1].'; % weight vector at
% sin(DOA) = 0.1
theta = pi*[-1/2:.00005:1/2]; % range of angles to compute response at
gamma = exp(-j*2*pi*d/lambda*sin(theta)); % form of array response
% vector element
D = (ones(n,1)*gamma).^([0:n-1].'*ones(1,max(size(gamma))))); % array
% response vectors
%
% add a Hamming taper to the beamformer weights
%k = -10:9;
%wh = .54 + .46*cos(pi*k/10);
%w_tap = wh.'.*w;
%r = w_tap'*D;
%
r = w'*D; % responses
plot(sin(theta),10*log10(abs(r).^2))
grid

%plotnb.m
% n is the number of sensors, N is the number of angles minus one,
% d is the interelement spacing, lam is the wavelength, and w is the
% weight vector
function [R] = plotnb(n,N,d,lam,w)
theta = pi/N*(0:N)-pi/2;
D = (ones(n,1)*(exp(-j*2*pi*d/lam*sin(theta)))).^([0:n-1].'*ones(1,N+1));
R = w'*D;
plot(sin(theta),10*log10(abs(R).^2))
grid
xlabel('sin of DOA')
ylabel('Gain in dB')

%plotfftnb.m
% N is the number of points in the FFT and w is the weight vector
function [R] = plotfftnb(N,w)
R = fftshift(fft(conj(w),N)); % N point FFT of conjugate of weight vector
R(N+1) = R(1); % add one point to response to enable plotting from -1
% to +1
k = [-1:1/(N/2):1]; % range of values for sin(theta)
plot(k,10*log10(abs(R).^2)) % plot gain of response vs sin(theta)
grid
xlabel('sin of DOA')
ylabel('Gain in dB')
```

```

%bfnb9s.m
clear
n = 20; % number of elements
% m = 200; % number of data vectors
lambda = 2; % wavelength
%sigma = 1e-3; % standard deviation of the noise
sigma_sq = 1e-6; % variance or power of noise
R_aa = eye(9); % spatial correlation matrix of signal-in-space vector
%
% decomposition of R_aa
%[v,e] = eig(R_aa);
%A = v*sqrt(e)*v';
%
%M = sigma*randn(n,m); % m noise vectors
d = 1; % interelement spacing
%
% array response vectors of signal and interferers
ds = exp(-j*2*pi*d/lambda*(0.1)) .* ([0:n-1].');
di1 = exp(-j*2*pi*d/lambda*(-.85)) .* ([0:n-1].');
di2 = exp(-j*2*pi*d/lambda*(-.55)) .* ([0:n-1].');
di3 = exp(-j*2*pi*d/lambda*(-.25)) .* ([0:n-1].');
di4 = exp(-j*2*pi*d/lambda*(0.05)) .* ([0:n-1].');
di5 = exp(-j*2*pi*d/lambda*(0.25)) .* ([0:n-1].');
di6 = exp(-j*2*pi*d/lambda*(0.45)) .* ([0:n-1].');
di7 = exp(-j*2*pi*d/lambda*(0.65)) .* ([0:n-1].');
di8 = exp(-j*2*pi*d/lambda*(0.85)) .* ([0:n-1].');
%
c = ds; % constraint
f = 1; % desired response
w_o = c*inv(c'*c)*f; % quiescent weight vector
%
% make C_n orthogonal to c and w_o
cc = [c w_o];
[U,S,V] = svd(cc);
C_n = U(:,2:n);
C_n'*c
C_n'*w_o
%
H = [ds di1 di2 di3 di4 di5 di6 di7 di8]; % direction matrix
%X = H*A*randn(9,m) + M; % m data vectors
%R_xx_hat = 1/m*X*X'; % sample covariance matrix
R_xx = H*R_aa*H' + sigma_sq*eye(n); % data covariance matrix
%norm(R_xx_hat - R_xx)
RI = inv(R_xx); % inverse of R_xx
w = RI*c*inv(c'*RI*c)*f; % optimum weight vector
w_n = inv(C_n'*R_xx*C_n)*C_n'*R_xx*w_o; % adaptive weights
w2 = w_o - C_n*w_n; % weight vector in GSC form
%RIh = inv(R_xx_hat);
%wh = RIh*c*inv(c'*RIh*c)*f;
figure(1)

```

```

%plotftnb2(1024,w,wh);
plotftnb(1024,w);
figure(2)
plotnb(n,10000,d,lambd,w);
figure(3)
plotnb(n,10000,d,lambd,w2);
figure(1)

```

```

%plotftwb.m

```

```

% K is the number of sensors, L is the number of taps per sensor, N is
% the number of points in the 2-dimensional FFT, f is the frequency,
% and w is the weight vector
function [R] = plotftwb(K,L,N,f,w)
W = reshape(w,K,L); % unstack the weight vector in a matrix where the
% columns are delayed array output vectors
R = fftshift(fft2(conj(W),N,N)); %2-dimensional FFT of conjugate of
% weight matrix
%
% add another row and column to allow plotting sin(theta) from -1 to
% +1 and normalized radian frequency from -pi to +pi radians
R(:,N+1) = R(:,1);
R(N+1,:) = R(1,:);
%
% determine how many points to use based on the frequency
fn = round(N*(f+.5)+1); % frequency number
ls = (N+1)-(fn+1)+1;
incs = floor((fn-(ls+1)+1)/2);
k = [-1:1/incs:1];
%
plot(k,10*log10(abs(R(ls+1:fn,fn)).^2)) % pull out column
% corresponding to frequency number and rows corresponding to good
% spatial points
grid
xlabel('sin of DOA')
ylabel('Gain in dB')

```

```

%mscmnew.m

```

```

% K is the number of sensors, L is the number of taps per sensor, the
% is the angle the source is arriving from, f1 and f2 are the lower
% and upper limits of the normalized frequency of the source, doc is
% the interelement spacing divided by the speed of propagation
function [R] = mscmnew(K,L,the,f1,f2,doc)
wb = 2*pi*f2; % normalized radian frequency
wa = 2*pi*f1; % normalized radian frequency
th = the*pi/180; % angle in radians
x = doc*sin(th);
R = zeros(K*L,K*L); % form data covariance matrix with all zeros
for i1 = -L+1:L-1; % for each value of i1, compute row and column
    for i2 = 0:K-1; % find row and column of matrix for each i1
        row(1,i2+1) = (1/(2*pi))*(wb*msinc(wb*(i1+i2*x))-wa*msinc(wa*(i1+i2*x)));
        col(1,i2+1) = (1/(2*pi))*(wb*msinc(wb*(i1-i2*x))-wa*msinc(wa*(i1-i2*x)));
    end
end

```

```

end
Rsub = toeplitz(col,row); %form toeplitz matrix
if i1 == 0;
    R = R + kron(eye(L),Rsub); % add matrices to main diagonal
elseif i1 > 0;
    % add matrices to diagonal above main diagonal
    R = R + kron(diag(ones(1,L-i1),i1),Rsub);
elseif i1 < 0;
    % add matrices to diagonal below main diagonal
    R = R + kron(diag(ones(1,L+i1),i1),Rsub);
end
end

%R_intur.m
% Ni is the number of frequency increments, th1 is angle of first
% source, th2 is the angle of the second source, f1 and f2 are the
% lower and upper frequencies of the sources, sig1_sq and sig2_sq are
% the variances or powers of the first and second sources
function [RI] = R_intur(K,L,Ni,th1,th2,f1,f2,sig1_sq,sig2_sq)
omega1 = 2*pi*f1;
omega2 = 2*pi*f2;
inc = (omega2 - omega1)/Ni; % find frequency increment
omega = omega1 + inc*(0:Ni); % frequency points
theta1 = th1*pi/180;
theta2 = th2*pi/180;
d1 = zeros(K*L,Ni+1); % set array response vectors of source 1 to zeros
d2 = zeros(K*L,Ni+1); % set array response vectors of source 1 to zeros
%
% for each frequency compute the array response vector of the sources
for i1 = 1:Ni+1;
    d1(:,i1)=kron(exp(-j*omega(i1)).^([0:L-1].')), ...
    exp(j*omega(i1)*sin(theta1)).^([(K-1)/2:-1:((K-1)/2)-K+1].'));
    d2(:,i1)=kron(exp(-j*omega(i1)).^([0:L-1].')), ...
    exp(j*omega(i1)*sin(theta2)).^([(K-1)/2:-1:((K-1)/2)-K+1].'));
end
%
A1 = d1;
A2 = d2;
Gam_sq = 0.5*eye(Ni+1)*inc; % flat PSD for real data
R_aa = [Gam_sq zeros(Ni+1,Ni+1);zeros(Ni+1,Ni+1) Gam_sq];
% covariance matrix over positive frequency for two uncorrelated sources
RIp = [sig1_sq*A1 sig2_sq*A2]*R_aa*[A1'; A2'];
% covariance matrix over negative frequency for two uncorrelated sources
RIm = [sig1_sq*conj(A1) sig2_sq*conj(A2)]*R_aa*[A1.'; A2.'];
RI = RIp + RIm; % covariance matrix for two uncorrelated sources

%Rdb.m
% oa and ob are the lower and upper radian frequencies, th1 and th2
% are the lower and upper angles of the source, Ni is the number of

```

```

% angle increments, i1 and i2 are indices from Rtdb.m
function [R] = Rdb(oa,ob,th1,th2,wi,i1,i2)
inc = (th2-th1)/wi; % angle increment
theta = th1 + inc*(0:wi); % angles
R = 0;
% approximate integral by Riemann sum at each angle; take care of
% cases when denominator could be zero
for ii = 1:wi+1;
    if i1-i2*sin(theta(ii)) == 0 & i1+i2*sin(theta(ii)) == 0;
        R = R + 2*(ob-oa)*inc;
    elseif i1-i2*sin(theta(ii)) == 0;
        R = R + ((ob-oa) + (exp(j*ob*(i1+i2*sin(theta(ii)))) - ...
exp(j*oa*(i1+i2*sin(theta(ii)))))/(j*(i1+i2*sin(theta(ii))))) * inc;
    elseif i1+i2*sin(theta(ii)) == 0;
        R = R + ((exp(-j*oa*(i1-i2*sin(theta(ii)))) - ...
exp(-j*ob*(i1-i2*sin(theta(ii)))))/(j*(i1-i2*sin(theta(ii))))) * inc;
    else
        R = R + ((exp(-j*oa*(i1-i2*sin(theta(ii)))) - ...
exp(-j*ob*(i1-i2*sin(theta(ii)))))/(j*(i1-i2*sin(theta(ii)))) + ...
exp(j*ob*(i1+i2*sin(theta(ii)))) - exp(j*oa*(i1+i2*sin(theta(ii)))))/(j*(i1+i2*sin(theta(ii))))) * inc;
    end
end
R = R/(4*pi);

%Rtdb.m
% the1 and the2 are the lower and upper angle limits of the source, f1
% and f2 are the lower and upper frequency limits of the source. and
% doc is the interelement spacing divided by the speed of propagation
function [R] = Rtdb(K,L,the1,the2,f1,f2,doc)
wb = 2*pi*f2;
wa = 2*pi*f1;
th1 = the1*pi/180;
th2 = the2*pi/180;
R = zeros(K*L,K*L);
for i1 = -L+1:L-1; % for each value of i1, compute row and column
    for i2 = 0:K-1; % find row and column of matrix for each i1
        row(1,i2+1) = Rdb(wa,wb,th1,th2,100,i1,i2);
        col(1,i2+1) = Rdb(wa,wb,th1,th2,100,i1,-i2);
    end
    Rsub = toeplitz(col,row);
    if i1 == 0;
        R = R + kron(eye(L),Rsub); % add matrices to main diagonal
    elseif i1 > 0;
        % add matrices to diagonal above main diagonal
        R = R + kron(diag(ones(1,L-i1),i1),Rsub);
    elseif i1 < 0;
        % add matrices to diagonal below main diagonal
        R = R + kron(diag(ones(1,L+i1),i1),Rsub);
    end
end

```

end

%bfbbrefern.m

clear

K = 16; % number of sensors

L = 5; % number of taps per sensor

f1 = .2;

f2 = .4;

doc = 1; % interelement spacing divided by speed of propagation

c_ang = -45; % constraint angle in degrees

sign_sq = .01; % noise variance or power

sig1_sq = 1; % variance or power of signal 1

sig2_sq = 1; % variance or power of signal 2

R_theta1 = mscmnew(K,L,45,f1,f2,doc);

R_theta2 = mscmnew(K,L,-45,f1,f2,doc);

% low rank approximation of R_theta1 and R_theta2

%

[U1,S1,V1] = svd(R_theta1);

eigen1 = svd(R_theta1);

[D1,per_en1] = getD(K,L,eigen1,.9999)

U_L1 = U1(:,1:D1);

S_L1 = S1(1:D1,1:D1);

V_L1 = V1(:,1:D1);

[U2,S2,V2] = svd(R_theta2);

eigen2 = svd(R_theta2);

[D2,per_en2] = getD(K,L,eigen2,.9999)

D2 = D1 % ensure matrix sizes are same

U_L2 = U2(:,1:D2);

S_L2 = S2(1:D2,1:D2);

V_L2 = V2(:,1:D2);

A1 = U_L1;

Sig11 = S_L1;

A2 = U_L2;

Sig22 = S_L2;

%

%

% another way to get square roots of matrices

%[v1,e1] = eig(Sig11);

%Sig11_sr = v1*sqrt(e1)*v1';

%[v2,e2] = eig(Sig22);

%Sig22_sr = v2*sqrt(e2)*v2';

%Sig12 = Sig11_sr*Sig22_sr;

%

Sig12 = sqrt(Sig11)*sqrt(Sig22);

Sig21 = conj(Sig12);

%Sig12 = zeros(size(Sig11)); % make uncorrelated for testing purposes

%Sig21 = zeros(size(Sig22)); % make uncorrelated for testing purposes

R_ss = [A1 A2]*[Sig11 Sig12;Sig21 Sig22]*[A1';A2']; % signal covariance

R_xx = R_ss + sign_sq*eye(K*L);

%R_xx = sig1_sq*R_theta1 + sig2_sq*R_theta2 + sign_sq*eye(K*L); % for

% uncorrelated testing

```

%
% compute eigenvector constraints
R_thetac = mscnnew(K,L,c_ang,f1,f2,doc);
eigen = svd(R_thetac);
[D,per_en] = getD(K,L,eigen,.9999)
[U,S,V] = svd(R_thetac);
U_L = U(:,1:D);
S_L = S(1:D,1:D);
V_L = V(:,1:D);
C = V_L;
fi = myfcen(K,L,c_ang,f1,f2,doc);
f = inv(S_L)*U_L'*fi;
w_o = C*inv(C'*C)*f;
RINV = inv(R_xx);
w = RINV*C*inv(C'*RINV*C)*f;
figure(1)
plotwb2d(K,L,1024,.2,w);
hold
plotwb2d(K,L,1024,.225,w);
plotwb2d(K,L,1024,.25,w);
plotwb2d(K,L,1024,.275,w);
plotwb2d(K,L,1024,.3,w);
plotwb2d(K,L,1024,.325,w);
plotwb2d(K,L,1024,.35,w);
plotwb2d(K,L,1024,.375,w);
plotwb2d(K,L,1024,.4,w);
hold
%figure(2)
%plotwb2d(K,L,1024,.2,w);
%figure(3)
%plotwb2d(K,L,1024,.3,w);
%figure(4)
%plotwb2d(K,L,1024,.4,w);
%[vo1,eo1] = eig(S1);
%S1_sr = vo1*sqrt(eo1)*vo1';
%[vo2,eo2] = eig(S2);
%S2_sr = vo2*sqrt(eo2)*vo2';
%for fj = .2:.025:.4;
% out_p = w'*U1*diag(sqrt(S1))
% out_m = w'*U2*diag(sqrt(S2))
% out_p = w'*U1*diag(sqrt(S1))*1
% out_m = w'*U2*diag(sqrt(S2))*rc*exp(-j*2*pi*fj*del)
% out_t = out_p + out_m
% abs(out_t)
% outdb_t = 10*log10(abs(out_t))
%end
%out_p = w'*U1*diag(sqrt(S1))*1
%out_m = w'*U2*diag(sqrt(S2))*rc*exp(-j*2*pi*.3*del)
%out_t = out_p + out_m
%abs(out_t)
%outdb_t = 10*log10(abs(out_t))

```

```

out_pow = w'*R_ss*w
abs(out_pow)
10*log10(abs(out_pow))
figure(1)

```

```

function [f] = myfcen(K,L,the,f1,f2,doc)
wb = 2*pi*f2;
wa = 2*pi*f1;
th = the*pi/180;
x = doc*sin(th);
R = zeros(1,K*L);
ii = 0;
for i1 = (L-1)/2:-1:((L-1)/2)-L+1;
    for i2 = (K-1)/2:-1:((K-1)/2)-K+1;
        ii = ii + 1;
        fr(ii) = (1/(2*pi))*(wb*msinc(wb*(i1+i2*x))-wa*msinc(wa*(i1+i2*x)));
    end
end
f = fr.';

```

```

function [answer] = msinc(x)
top = length(x);
for ii = 1:top;
    if x(ii) == 0;
        answer(ii) = 1;
    else
        answer(ii) = sin(x(ii))/x(ii);
    end
end
end

```

```

%myfcenref.m
function [f] = myfcenref(K,L,the,f1,f2,doc,P)
wb = 2*pi*f2;
wa = 2*pi*f1;
th = the*pi/180;
x = doc*sin(th);
R = zeros(1,K*L);
ii = 0;
for i1 = (L-1)/2:-1:((L-1)/2)-L+1;
    for i2 = (K-1)/2:-1:((K-1)/2)-K+1;
        ii = ii + 1;
        fr(ii) = (1/(2*pi))*(wb*msinc(wb*(i1+(P*sin(th))+i2*x))- ...
            wa*msinc(wa*(i1+(P*sin(th))+i2*x)));
    end
end
f = fr.';

```

```

%ftdb.m
function [f] = ftdb(K,L,the1,the2,f1,f2,doc)
wb = 2*pi*f2;
wa = 2*pi*f1;

```

```

th1 = the1*pi/180;
th2 = the2*pi/180;
R = zeros(1,K*L);
ii = 0;
for i1 = (L-1)/2:-1:((L-1)/2)-L+1;
    for i2 = (K-1)/2:-1:((K-1)/2)-K+1;
        ii = ii + 1;
        fr(ii) = fdb(wa,wb,th1,th2,100,i1,i2) + fdb(wa,wb,th1,th2,100,i1,-i2);
    end
end
f = fr.';

%fdb.m
function [f] = fdb(oa,ob,th1,th2,ni,i1,i2)
inc = (th2-th1)/ni;
theta = th1 + inc*(0:ni);
f = 0;
for ii = 1:ni+1;
    if i1+i2*sin(theta(ii)) == 0;
        f = f + 2*(ob-oa)*inc;
    else
        f = f+((exp(j*ob*(i1+i2*sin(theta(ii))))- ...
exp(j*oa*(i1+i2*sin(theta(ii)))))/(j*(i1+i2*sin(theta(ii))))+ ...
(exp(-j*ob*(i1+i2*sin(theta(ii))))-exp(-j*oa*(i1+i2*sin(theta(ii)))))/ ...
(-j*(i1+i2*sin(theta(ii)))))*inc;
    end
end
f = f/(8*pi);

%bfb4_23d.m
clear
L = 5;
K = 16;
doc = 1;
c_ang = 18;
f1 = .2;
f2 = .4;
sign_sq = .01;
sig1_sq = 10;
sig2_sq = 100;
R_theta1 = mscmnew(K,L,-17.5,f1,f2,doc);
R_theta2 = mscmnew(K,L,-5.75,f1,f2,doc);
RI = R_intur(K,L,100,-17.5,-5.75,f1,f2,sig1_sq,sig2_sq);
norm(RI-(sig1_sq*R_theta1 + sig2_sq*R_theta2))
R_thetac = mscmnew(K,L,c_ang,f1,f2,doc);
eigen = svd(R_thetac)
[D,per_en] = getD(K,L,eigen,.9999)
%D = ceil(((K-1)*(sin(c_ang*pi/180))+L-1)*2*(f2-f1)+1)
%per_en = sum(eigen(1:D,1))/sum(eigen)
R_xx = sig1_sq*R_theta1 + sig2_sq*R_theta2 + sign_sq*eye(K*L);
R_xxn = RI + sign_sq*eye(K*L);

```

```

[U,S,V] = svd(R_thetac);
U_L = U(:,1:D);
S_L = S(1:D,1:D);
V_L = V(:,1:D);
C = V_L;
fi = myfcen(K,L,c_ang,f1,f2,doc);
f = inv(S_L)*U_L'*fi;
w_o = C*inv(C'*C)*f;
CC = [C w_o];
[UU,SS,VV] = svd(CC);
C_n = UU(:,D+1:K*L);
C_n'*C
C_n'*w_o
D
per_en
w_n = inv(C_n'*R_xx*C_n)*C_n'*R_xx*w_o;
w2 = w_o - C_n*w_n;
RINV = inv(R_xx);
RINVn = inv(R_xxn);
w1 = RINV*C*inv(C'*RINV*C)*f;
wn = RINVn*C*inv(C'*RINVn*C)*f;
%figure(1)
%plotfftwb2(K,L,512,.3,w1,wn);
%figure(2)
%plotfftwb2(K,L,512,.3,w1,w2);
%figure(3)
%plotwb2d2(K,L,1024,.3,w1,wn);
%figure(2)
%plotwb2d2(K,L,1024,.3,w1,w2);
figure(1)
%plotwb2d(K,L,1024,.3,w_o);
plotwb2d(K,L,1024,.2,w1);
hold
plotwb2d(K,L,1024,.225,w1);
plotwb2d(K,L,1024,.25,w1);
plotwb2d(K,L,1024,.275,w1);
plotwb2d(K,L,1024,.3,w1);
plotwb2d(K,L,1024,.325,w1);
plotwb2d(K,L,1024,.35,w1);
plotwb2d(K,L,1024,.375,w1);
plotwb2d(K,L,1024,.4,w1);
hold
figure(2)
plotwb3d(K,L,32,w1);
%figure(2)
%plotwb2d2(K,L,1024,.3,w1,w2);
%figure(3)
%plotgf1(K,L,1024,c_ang,w_o);
figure(4)
plotgf1(K,L,1024,-17.5,w1);
hold

```

```

plotgf1(K,L,1024,-5.75,w1);
hold
figure(5)
plotpf1(K,L,1024,c_ang,w_o);
figure(1)

```

```

%plotwb3d.m
function [R] = plotwb3d(K,L,N,w)
omega = 2*pi/N*(0:N) - pi;
theta = pi/N*(0:N) - pi/2;
R = zeros(N+1,N+1);
d = zeros(K*L*(N+1),N+1);
for i1 = 1:N+1;
    for i2 = 1:N+1;
        d(1+(i1-1)*K*L:i1*K*L,i2)=kron(exp(-j*omega(i1)).^([0:L-1].')
            ,exp(j*omega(i1)*sin(theta(i2))).^([(K-1)/2:-1:((K-1)/2)-K+1].')));
    end
    R(i1,:) = w'*d(1+(i1-1)*K*L:i1*K*L,:);
end
meshc(theta*180/pi,omega,10*log10(abs(R).^2))
xlabel('DOA in degrees')
ylabel('Normalized f in rad')
zlabel('Gain in dB')

```

```

%bfbbf4_9.m
clear
L = 6;
K = 15;
f1 = .3;
f2 = .4;
doc = 1;
c_ang = 5.74;
R_thetac = mscmnew(K,L,c_ang,f1,f2,doc);
R_theta1 = mscmnew(K,L,23.58,f1,f2,doc);
R_theta2 = mscmnew(K,L,36.87,f1,f2,doc);
eigen = svd(R_thetac)
[D,per_en] = getD(K,L,eigen,.9999)
sign_sq = .01;
sig1_sq = 10;
sig2_sq = 100;
R_xx = sig1_sq*R_theta1 + sig2_sq*R_theta2 + sign_sq*eye(K*L);
[U,S,V] = svd(R_thetac);
U_L = U(:,1:D);
V_L = V(:,1:D);
S_L = S(1:D,1:D);
C = V_L;
f1 = myfcen(K,L,c_ang,f1,f2,doc);
f = inv(S_L)*U_L'*f1;
w_o = C*inv(C'*C)*f;
RI = inv(R_xx);
w = RI*C*inv(C'*RI*C)*f;

```

```

figure(1)
plotwb2d(K,L,1024,.3,w);
hold
plotwb2d(K,L,1024,.325,w);
plotwb2d(K,L,1024,.35,w);
plotwb2d(K,L,1024,.375,w);
plotwb2d(K,L,1024,.4,w);
hold
figure(2)
plotgf1(K,L,1024,c_ang,w_o);
figure(3)
plotpf1(K,L,1024,c_ang,w_o);
figure(4)
plotwb2d(K,L,1024,.3,w_o);
hold
plotwb2d(K,L,1024,.325,w_o);
plotwb2d(K,L,1024,.35,w_o);
plotwb2d(K,L,1024,.375,w_o);
plotwb2d(K,L,1024,.4,w_o);
hold
figure(1)

%bfbbadddb.m
clear
L = 5;
K = 16;
cod = 1;
c_ang = 0;
c_ang1 = -5;
c_ang2 = 0;
f1 = .2;
f2 = .4;
sign_sq = .01;
sig1_sq = 1;
sig2_sq = 1;
R_theta1 = Rtdb(K,L,30,35,f1,f2,1);
R_theta2 = Rtdb(K,L,40,45,f1,f2,1);
R_thetac = Rtdb(K,L,c_ang1,c_ang2,f1,f2,1);
R_thetac = mscmnew(K,L,c_ang,f1,f2,1);
eigen = svd(R_thetac)
%D,per_en] = getD(K,L,eigen,.87)
D = ceil(((K-1)*(sin(c_ang2*pi/180)-sin(c_ang1*pi/180))+L-1)*2*(f2-f1)+1)
per_en = sum(eigen(1:D,1))/sum(eigen)
R_xx = sig1_sq*R_theta1 + sig2_sq*R_theta2 + sign_sq*eye(K*L);
R_xxn = RI + sign_sq*eye(K*L);
R_xx = sig1_sq*R_theta1 + sign_sq*eye(K*L);
R_xx = sign_sq*eye(K*L);
[U,S,V] = svd(R_thetac);
U_L = U(:,1:D);
S_L = S(1:D,1:D);
V_L = V(:,1:D);

```

```

C = V_L;
fi = ftdb(K,L,c_ang1,c_ang2,f1,f2,1);
%fi = myfcen(K,L,c_ang,f1,f2,1);
f = inv(S_L)*U_L'*fi;
w_o = C*inv(C'*C)*f;
RINV = inv(R_xx);
%RINVn = inv(R_xxn);
w = RINV*C*inv(C'*RINV*C)*f;
%wn = RINVn*C*inv(C'*RINVn*C)*f;
%figure(1)
%plotfftwb(K,L,512,.3,w);
%figure(2)
%plotwb2d(K,L,1024,.2,w);
%hold
%plotwb2d(K,L,1024,.225,w);
%plotwb2d(K,L,1024,.25,w);
%plotwb2d(K,L,1024,.275,w);
%plotwb2d(K,L,1024,.3,w);
%plotwb2d(K,L,1024,.325,w);
%plotwb2d(K,L,1024,.35,w);
%plotwb2d(K,L,1024,.375,w);
%plotwb2d(K,L,1024,.4,w);
%hold
figure(3)
plotmf1(K,L,1024,((c_ang1+c_ang2)/2),w);
figure(4)
plotpf1(K,L,1024,((c_ang1+c_ang2)/2),w);
figure(1)

%bfbbreftnn.m
clear
K = 16;
L = 15;
f1 = .2;
f2 = .3;
cod = 1;
c_ang = -45;
P = 9;
rc = .5;
sign_sq = .01;
R_11 = mscmnew(K,L,45,f1,f2,cod);
R_21 = mscm21h(K,L,45,f1,f2,cod,P);
R_12 = mscm12h(K,L,45,f1,f2,cod,P);
R_22 = mscm22(K,L,45,f1,f2,cod);
%R_22 = mscmnew(K,L,-45,f1,f2,cod);
R_xx = R_11 + rc*R_21 + rc*R_12 + (rc.^2)*R_22 + sign_sq*eye(K*L);
R_thetac = mscmnew(K,L,c_ang,f1,f2,cod);
eigen = svd(R_thetac);
[D,per_en] = getD(K,L,eigen,.9999)
[U,S,V] = svd(R_thetac);
U_L = U(:,1:D);

```

```

S_L = S(1:D,1:D);
V_L = V(:,1:D);
C = V_L;
fi = myfcenref(K,L,c_ang,f1,f2,cod,P);
f = inv(S_L)*U_L'*fi;
w_o = C*inv(C'*C)*f;
RINV = inv(R_xx);
w = RINV*C*inv(C'*RINV*C)*f;
figure(1)
plotwb2d(K,L,1024,.2,w);
hold
plotwb2d(K,L,1024,.225,w);
plotwb2d(K,L,1024,.25,w);
plotwb2d(K,L,1024,.275,w);
plotwb2d(K,L,1024,.3,w);
plotwb2d(K,L,1024,.325,w);
plotwb2d(K,L,1024,.35,w);
plotwb2d(K,L,1024,.375,w);
plotwb2d(K,L,1024,.4,w);
hold
%plotwb2d(K,L,1024,.3,w);
out_p = w'*R_xx*w
10*log10(out_p)

%outputpownbq.m
clear
d = 1;
n = 16;
lambda = 2;
sigman_sq = 1e-6;
rc = .25;
P = 8;
del = 2*P*.707;
R_aa = [1 rc*exp(j*2*pi/lambda*del*d); ...
        rc*exp(-j*2*pi/lambda*del*d) rc.^2];
did = exp(j*2*pi*d/lambda*(0.707)).^([(n-1)/2:-1:((n-1)/2)-n+1].');
dii = exp(j*2*pi*d/lambda*(-0.707)).^([(n-1)/2:-1:((n-1)/2)-n+1].');
ds = exp(j*2*pi*d/lambda*(-0.707)).^([(n-1)/2:-1:((n-1)/2)-n+1].');
c = ds;
f = 1;
w_o = c*inv(c'*c)*f;
cc = [c w_o];
[U,S,V] = svd(cc);
C_n = U(:,2:n);
C_n'*c
C_n'*w_o
H = [dii dii];
R_xx = H*R_aa*H' + sigman_sq*eye(n);
RI = inv(R_xx);
w1 = RI*c*inv(c'*RI*c)*f;
w_n = inv(C_n'*R_xx*C_n)*C_n'*R_xx*w_o;

```

```

w2 = w_o - C_n*w_n;
op = zeros(181,1);
opdb = zeros(181,1);
for ang = -90:90;
    angr = ang*pi/180;
    di = exp(-j*2*pi*d/lambda*sin(angr)) .* ([0:n-1].');
    H = [di];
    Rx = H*H' + sigman_sq*eye(n);
    op(ang+91) = w_o'*Rx*w_o;
    opdb(ang+91) = 10*log10(op(ang+91));
end
for ang = 1:90;
    angr = ang*pi/180;
    rc = (angr^2)/((pi/2)^2);
    del = 2*P*sin(angr);
    R_aa = [1 rc*exp(j*2*pi/lambda*del*d); ...
            rc*exp(-j*2*pi/lambda*del*d) rc.^2];
    did = exp(j*2*pi*d/lambda*sin(angr)).^([(n-1)/2:-1:((n-1)/2)-n+1].');
    dii = exp(j*2*pi*d/lambda*sin(-angr)).^([(n-1)/2:-1:((n-1)/2)-n+1].');
    H = [did dii];
    Rx = H*R_aa*H' + sigman_sq*eye(n);
    op(ang+91) = w_o'*Rx*w_o;
    opdb(ang+91) = 10*log10(op(ang+91));
end
angles = [-90:90];
plot(angles,10*log10(abs(op)))
xlabel('DOA')
ylabel('Output Power in dB with Quiescent Weights')

%outputpownbw.m
clear
d = 1;
n = 16;
lambda = 2;
sigman_sq = 1e-6;
rc = .25;
P = 8;
del = 2*P*.707;
R_aa = [1 rc*exp(j*2*pi/lambda*del*d); ...
        rc*exp(-j*2*pi/lambda*del*d) rc.^2];
did = exp(j*2*pi*d/lambda*(0.707)).^([(n-1)/2:-1:((n-1)/2)-n+1].');
dii = exp(j*2*pi*d/lambda*(-0.707)).^([(n-1)/2:-1:((n-1)/2)-n+1].');
ds = exp(j*2*pi*d/lambda*(-0.707)).^([(n-1)/2:-1:((n-1)/2)-n+1].');
c = ds;
f = 1;
w_o = c*inv(c'*c)*f;
cc = [c w_o];
[U,S,V] = svd(cc);
C_n = U(:,2:n);
C_n'*c
C_n'*w_o

```

```

H = [did dii];
R_xx = H*R_aa*H' + sigman_sq*eye(n);
RI = inv(R_xx);
w1 = RI*c*inv(c'*RI*c)*f;
w_n = inv(C_n'*R_xx*C_n)*C_n'*R_xx*w_o;
w2 = w_o - C_n*w_n;
op = zeros(181,1);
opdb = zeros(181,1);
for ang = -90:0;
    angr = ang*pi/180;
    di = exp(-j*2*pi*d/lambda*sin(angr)) .^ ([0:n-1].');
    H = [di];
    Rx = H*H' + sigman_sq*eye(n);
    op(ang+91) = w2'*Rx*w2;
    opdb(ang+91) = 10*log10(op(ang+91));
end
for ang = 1:90;
    angr = ang*pi/180;
    rc = (angr^2)/((pi/2)^2);
    del = 2*P*sin(angr);
    R_aa = [1 rc*exp(j*2*pi/lambda*del*d); ...
            rc*exp(-j*2*pi/lambda*del*d) rc.^2];
    did = exp(j*2*pi*d/lambda*sin(angr)).^([(n-1)/2:-1:(n-1)/2-n+1].');
    dii = exp(j*2*pi*d/lambda*sin(-angr)).^([(n-1)/2:-1:(n-1)/2-n+1].');
    H = [did dii];
    Rx = H*R_aa*H' + sigman_sq*eye(n);
    op(ang+91) = w2'*Rx*w2;
    opdb(ang+91) = 10*log10(op(ang+91));
end
angles = [-90:90];
plot(angles,10*log10(abs(op)))
xlabel('DOA')
ylabel('Output Power in dB with Adapted Weights')

%outputpowq.m
K = 16;
L = 25;
f1 = .3;
f2 = .4;
doc = 1;
c_ang = -45;
ang = 45;
P = 9;
rc = 0.25;
sign_sq = .01;
R_11 = mscmnew(K,L,ang,f1,f2,doc);
R_21 = mscm21h(K,L,ang,f1,f2,doc,P);
R_12 = mscm12h(K,L,ang,f1,f2,doc,P);
R_22 = mscm22(K,L,ang,f1,f2,doc);
R_thetac = mscmnew(K,L,c_ang,f1,f2,doc);
R_xx = R_11 + rc*R_21 + rc*R_12 + (rc.^2)*R_22 + sign_sq*eye(K*L);

```

```

eigen = svd(R_thetac);
[D,per_en] = getD(K,L,eigen,.9999);
[U,S,V] = svd(R_thetac);
U_L = U(:,1:D);
S_L = S(1:D,1:D);
V_L = V(:,1:D);
C = V_L;
fi = myfcenref(K,L,c_ang,f1,f2,doc,P);
f = inv(S_L)*U_L'*fi;
w_o = C*inv(C'*C)*f;
CC = [C w_o];
[UU,SS,VV] = svd(CC);
C_n = UU(:,D+1:K*L);
w_n = inv(C_n'*R_xx*C_n)*C_n'*R_xx*w_o;
w2 = w_o - C_n*w_n;
RINV = inv(R_xx);
w = RINV*C*inv(C'*RINV*C)*f;
op = zeros(181,1);
opdb = zeros(181,1);
for ang = -90:0;
    R = mscmnew(16,L,ang,f1,f2,doc);
    Rx = R + sign_sq*eye(K*L);
    op(ang+91) = w_o'*Rx*w_o;
    opdb(ang+91) = 10*log10(op(ang+91));
end
for ang = 1:90;
    angr = ang*pi/180;
    rc = (angr^2)/((pi/2)^2)
    R_11 = mscmnew(K,L,ang,f1,f2,doc);
    R_21 = mscm21h(K,L,ang,f1,f2,doc,P);
    R_12 = mscm12h(K,L,ang,f1,f2,doc,P);
    R_22 = mscm22(K,L,ang,f1,f2,doc);
    Rx = R_11 + rc*R_21 + rc*R_12 + (rc^2)*R_22 + sign_sq*eye(K*L);
    op(ang+91) = w_o'*Rx*w_o;
    opdb(ang+91) = 10*log10(op(ang+91));
end
opmax = max(op);
opnorm = op/opmax;
angles = [-90:90];
plot(angles,10*log10(opmax))
xlabel('DOA')
ylabel('Normalized Output Power in dB with Quiescent Weights')

%outputpow.m
K = 16;
L = 25;
f1 = .3;
f2 = .4;
doc = 1;
c_ang = -45;
ang = 45;

```

```

P = 9;
rc = 0.25;
sign_sq = .01;
R_11 = mscmnew(K,L,ang,f1,f2,doc);
R_21 = mscm21h(K,L,ang,f1,f2,doc,P);
R_12 = mscm12h(K,L,ang,f1,f2,doc,P);
R_22 = mscm22(K,L,ang,f1,f2,doc);
R_thetac = mscmnew(K,L,c_ang,f1,f2,doc);
R_xx = R_11 + rc*R_21 + rc*R_12 + (rc.^2)*R_22 + sign_sq*eye(K*L);
eigen = svd(R_thetac);
[D,per_en] = getD(K,L,eigen,.9999);
[U,S,V] = svd(R_thetac);
U_L = U(:,1:D);
S_L = S(1:D,1:D);
V_L = V(:,1:D);
C = V_L;
fi = myfcenref(K,L,c_ang,f1,f2,doc,P);
f = inv(S_L)*U_L'*fi;
w_o = C*inv(C'*C)*f;
CC = [C w_o];
[UU,SS,VV] = svd(CC);
C_n = UU(:,D+1:K*L);
w_n = inv(C_n'*R_xx*C_n)*C_n'*R_xx*w_o;
w2 = w_o - C_n*w_n;
RINV = inv(R_xx);
w = RINV*C*inv(C'*RINV*C)*f;
op = zeros(181,1);
opdb = zeros(181,1);
for ang = -90:0;
    R = mscmnew(16,L,ang,f1,f2,doc);
    Rx = R + sign_sq*eye(K*L);
    op(ang+91) = w'*Rx*w;
    opdb(ang+91) = 10*log10(op(ang+91));
end
for ang = 1:90;
    angr = ang*pi/180;
    rc = (angr^2)/((pi/2)^2);
    R_11 = mscmnew(K,L,ang,f1,f2,doc);
    R_21 = mscm21h(K,L,ang,f1,f2,doc,P);
    R_12 = mscm12h(K,L,ang,f1,f2,doc,P);
    R_22 = mscm22(K,L,ang,f1,f2,doc);
    Rx = R_11 + rc*R_21 + rc*R_12 + (rc.^2)*R_22 + sign_sq*eye(K*L);
    op(ang+91) = w'*Rx*w;
    opdb(ang+91) = 10*log10(op(ang+91));
end
opmax = max(op);
opnorm = op/opmax;
angles = [-90:90];
plot(angles,10*log10(opmax))
xlabel('DOA')
ylabel('Normalized Output Power in dB with Adapted Weights')

```

Bibliography

1. Alexander, S. Thomas. *Adaptive Signal Processing: Theory and Applications*. New York: Springer-Verlag, Inc., 1986.
2. Applebaum, Sidney P. and Dean J. Chapman. "Adaptive Arrays with Main Beam Constraints," *IEEE Transactions on Antennas and Propagation*, 24(5) (September 1976).
3. Brennan, L. E., et al. *Adaptive Cancellation of Scattered Interference*. Technical Report AD-A141 566, Adaptive Sensors, Inc., March 1984.
4. Bresler, Yoram and others. "Optimum Beamforming for Coherent Signal and Interferences," *IEEE Transactions on Acoustics, Speech, and Signal Processing*, 36(6) (June 1988).
5. Buckley, Kevin M. "Spatial/Spectral Filtering with Linearly Constrained Minimum Variance Beamformers," *IEEE Transactions on Acoustics, Speech, and Signal Processing*, 35(3) (March 1987).
6. Buckley, Kevin M. and Lloyd J. Griffiths. "An Adaptive Generalized Sidelobe Canceller with Derivative Constraints," *IEEE Transactions on Antennas and Propagation*, 34(3) (March 1986).
7. Chapman, Dean J. "Partial Adaptivity for the Large Array," *IEEE Transactions on Antennas and Propagation*, 24(5) (September 1976).
8. Compton, R. T., Jr. *Adaptive Antennas: Concepts and Performance*. New Jersey: Prentice-Hall, Inc., 1988.
9. Compton, R. T., Jr. "The Bandwidth Performance of a Two-Element Adaptive Array with Tapped Delay-Line Processing," *IEEE Transactions on Antennas and Propagation*, 36(1) (January 1988).
10. Dudgeon, Dan E. "Fundamentals of Digital Array Processing." *Proceedings of the IEEE*. vol. 65, pp. 898-904. June 1977.
11. Dudgeon, Dan E. and Russell M. Mersereau. *Multidimensional Digital Signal Processing*. New Jersey: Prentice-Hall, Inc., 1984.
12. El-Ayadi, M. Hatim and others. "A Generalized Solution to the Adaptive Nulling Problem in the Presence of Coherent Jammers," *IEEE Transactions on Antennas and Propagation*, 40(12) (December 1992).
13. Er, Meng Hwa and Antonio Cantoni. "Derivative Constraints for Broad-Band Element Space Antenna Array Processors," *IEEE Transactions on Acoustics, Speech, and Signal Processing*, 31(6) (December 1983).
14. Er, Meng Hwa and Antonio Cantoni. "A New Set of Linear Constraints for Broad-Band Time Domain Element Space Processors," *IEEE Transactions on Antennas and Propagation*, 34(3) (March 1986).
15. Frost, Otis Lamont, III. "An Algorithm for Linearly Constrained Adaptive Array Processing." *Proceedings of the IEEE*. vol. 60, pp. 926-935. August 1972.
16. Gabriel, William F. "Using Spectral Estimation Techniques in Adaptive Processing Antenna Systems," *IEEE Transactions on Antennas and Propagation*, 34(3) (March 1986).
17. Godara, Lal Chand. "Beamforming in the Presence of Correlated Arrivals Using Structured Correlation Matrix," *IEEE Transactions on Acoustics, Speech, and Signal Processing*, 38(1) (January 1990).

18. Griffiths, L. J. "A Simple Adaptive Algorithm for Real-Time Processing in Antenna Arrays." *Array Processing Applications to Radar* edited by Simon Haykin, 192-200, Pennsylvania: Dowden, Hutchinson & Ross, Inc., 1980.
19. Griffiths, L. J. "A New Approach to Partially Adaptive Arrays." *ICASSP*. pp. 1999-2002. April 1987.
20. Griffiths, Lloyd J. and Kevin M. Buckley. "Quiescent Pattern Control in Linearly Constrained Adaptive Arrays," *IEEE Transactions on Acoustics, Speech, and Signal Processing*, 35(7) (July 1987).
21. Griffiths, Lloyd J. and Charles W. Jim. "An Alternative Approach to Linearly Constrained Adaptive Beamforming," *IEEE Transactions on Antennas and Propagation*, 30(1) (January 1982).
22. Hudson, J. E. *Adaptive Array Principles*. New York: Peter Peregrinus LTD, 1981.
23. Jablon, Neil K. "Steady State Analysis of the Generalized Sidelobe Canceller by Adaptive Noise Cancelling Techniques," *IEEE Transactions on Antennas and Propagation*, 34(3) (March 1986).
24. Justice, J. H. and others. *Array Signal Processing*. New Jersey: Prentice-Hall, Inc., 1985.
25. Li, Tze Fen and Sung Wu Chang. "A Quick Method for Estimation of Parameters of Individual Pulses in a Multipath Signal," *Pattern Recognition*, 25(12) (December 1992).
26. Liu, Tsung-Ching and Barry Van Veen. "A Modular Structure for Implementation of Linearly Constrained Minimum Variance Beamformers," *IEEE Transactions on Signal Processing*, 39(10) (October 1991).
27. Magnus, Jan R. and Heinz Neudecker. *Matrix differential Calculus with Applications in Statistics and Econometrics*. New York: John Wiley and Sons, 1988.
28. McWhirter, J. G. and others. "The Application of Linear Constraints to an Adaptive Beamformer." *ICASSP*. pp. 1881-1884. 1986.
29. Miedaner, Donald and Ping Li. *X-Band Air to Air, Sidelobe Clutter Mitigation Through Adaptive Processing: Radome Effects*. Technical Report WL-TR-92-1075, Adaptive Technology, Inc., June 1992.
30. Monzingo, R. A. and T. W. Miller. *Introduction to Adaptive Arrays*. New York: John Wiley & Sons, Inc., 1980.
31. Morgan, Dennis R. "Partially Adaptive Array Techniques," *IEEE Transactions on Antennas and Propagation*, 26(6) (November 1978).
32. Nitzberg, Ramon. *Adaptive Signal Processing for Radar*. Massachusetts: Artech House, Inc., 1992.
33. Park, Hyung Rae and Young-Soo Kim. "A Solution to the Narrow-Band Coherency Problem in Multiple Source Location," *IEEE Transactions on Signal Processing*, 41(1) (July 1980).
34. Reddy, V. Umapathi and others. "Performance Analysis of the Optimum Beamformer in the Presence of Correlated Sources and Its Behavior Under Spatial Smoothing," *IEEE Transactions on Acoustics, Speech, and Signal Processing*, 35(7) (July 1987).
35. Scharf, Louis L. *Statistical Signal Processing: Detection, Estimation, and Time Series Analysis*. Massachusetts: Addison-Wesley Publishing Company, Inc., 1991.
36. Shan, Tie-Jun and Thomas Kailath. "Adaptive Beamforming for Coherent Signals and Interference," *IEEE Transactions on Acoustics, Speech, and Signal Processing*, 33(3) (June 1985).

37. Shanmugan, K. Sam and Arthur M. Breipohl. *Random Signals: Detection, Estimation, and Data Analysis*. New York: John Wiley & Sons, Inc., 1988.
38. Tran, Jean-Marie Q. D. and William S. Hodgkiss. "Spatial Smoothing and Minimum Variance Beamforming on Data from Large Aperture Vertical Line Arrays," *IEEE Journal of Oceanic Engineering*, 18(1) (January 1993).
39. Van Veen, Barry. "An Analysis of Several Partially Adaptive Beamformer Designs," *IEEE Transactions on Acoustics, Speech, and Signal Processing*, 37(2) (February 1989).
40. Van Veen, Barry. "Minimum Variance Beamforming." *Adaptive Radar Detection and Estimation* edited by Simon Haykin and Allan Steinhardt, 161-236, New York: John Wiley & Sons, Inc., 1992.
41. Van Veen, Barry. "Improved Power Minimization Based Partially Adaptive Beamformer Design." *ICASSP*. pp. 2793-2796. April 1988.
42. Van Veen, Barry D. "Eigenstructure Based Partially Adaptive Array Design," *IEEE Transactions on Antennas and Propagation*, 37(3) (March 1988).
43. Van Veen, Barry D. "Optimization of Quiescent Response in Partially Adaptive Beamformers," *IEEE Transactions on Acoustics, Speech, and Signal Processing*, 38(3) (March 1990).
44. Van Veen, Barry D. "Minimum Variance Beamforming with Soft Response Constraints," *IEEE Transactions on Signal Processing*, 39(9) (September 1991).
45. Van Veen, Barry D. and Kevin M. Buckley. "Beamforming: A Versatile Approach to Spatial Filtering," *IEEE Transactions on Acoustics, Speech, and Signal Processing*, 5 (April 1988).
46. Van Veen, Barry D. and Richard A. Roberts. "An Adaptive Beamformer Design Via Output Power Minimization," *IEEE Transactions on Acoustics, Speech, and Signal Processing*, 35(11) (November 1987).
47. Vural, A. M. "A Comparative Performance Study of Adaptive Array Processors." *ICASSP*. pp. 695-700. April 1977.
48. Wang, H. and M. Kaveh. "Coherent Signal-Subspace Processing for the Detection and Estimation of Angles of Arrival of Multiple Wide-Band Sources," *IEEE Transactions on Acoustics, Speech, and Signal Processing*, 33(4) (August 1985).
49. Ward, James and R. T. Compton Jr. "Sidelobe Level Performance of Adaptive Sidelobe Canceller Arrays with Element Reuse," *IEEE Transactions on Antennas and Propagation*, 38(10) (October 1990).
50. White, Warren D. "Wideband Interference Cancellation in Adaptive Sidelobe Cancellers," *IEEE Transactions on Aerospace and Electronic Systems*, 19(6) (November 1983).
51. Widrow, Bernard and Samuel D. Stearns. *Adaptive Signal Processing*. New Jersey: Prentice-Hall, Inc., 1985.
52. Yang, J. F. and M. Kaveh. "Wideband Adaptive Arrays Based on the Coherent Signal-Subspace Transformation." *ICASSP*. pp. 2011-2014. April 1987.
53. Yeh, Chien-Chung and others. "On the Coherent Interference Suppression Using a Spatially Smoothing Adaptive Array," *IEEE Transactions on Antennas and Propagation*, 37(7) (July 1989).
54. Zhu, J. X. and H. Wang. "Adaptive Beamforming for Correlated Signal and Interference: A Frequency Domain Smoothing Approach," *IEEE Transactions on Acoustics, Speech, and Signal Processing*, 38(1) (January 1990).

Vita

Captain Mark Godino was born on 29 October 1960 in Belleville, New Jersey. He graduated from Bloomfield High School in Bloomfield, New Jersey in 1978 and attended Stevens Institute of Technology in Hoboken, New Jersey, graduating with a Bachelor of Engineering (specialty: Chemical Engineering) in May 1982. He attended Officer Training School from January 1983 until he was commissioned as a Second Lieutenant in the U.S. Air Force. His first assignment was at Ohio University as part of the Undergraduate Engineer Conversion Program. He graduated from Ohio University in November 1984 with a Bachelor of Science Degree in Electrical Engineering. He spent five years at the radar branch in the engineering directorate of Aeronautical Systems Division at Wright-Patterson AFB Ohio. While stationed in Ohio, he earned a Master of Science Degree in Management Science from the University of Dayton and attended Squadron Officer School in residence at Maxwell AFB, Alabama. He then worked for two years testing electronic warfare systems at the 513th Test Squadron in Strategic Air Command. In 1992, he was assigned to the Air Force Institute of Technology to earn his Master of Science Degree in Electrical Engineering.

Permanent address: 3152 Meadow Wood Drive
Springfield, Ohio 45505

REPORT DOCUMENTATION PAGE			Form Approved OMB No. 0704-0188	
Public reporting burden for this collection of information is estimated to average 1 hour per response, including the time for reviewing instructions, searching existing data sources, gathering and maintaining the data needed, and completing and reviewing the collection of information. Send comments regarding this burden estimate or any other aspect of this collection of information, including suggestions for reducing this burden, to Washington Headquarters Services, Directorate for Information Operations and Reports, 1215 Jefferson Davis Highway, Suite 1204, Arlington, VA 22202-4302, and to the Office of Management and Budget, Paperwork Reduction Project (0704-0188), Washington, DC 20503.				
1. AGENCY USE ONLY (Leave blank)		2. REPORT DATE December 1993		3. REPORT TYPE AND DATES COVERED Master's Thesis
4. TITLE AND SUBTITLE ANALYZING ADAPTIVE BEAMFORMER PERFORMANCE IN A STABLE MULTIPATH ENVIRONMENT			5. FUNDING NUMBERS	
6. AUTHOR(S) Mark Godino, Capt, USAF				
7. PERFORMING ORGANIZATION NAME(S) AND ADDRESS(ES) Air Force Institute of Technology, WPAFB OH 45433-6583			8. PERFORMING ORGANIZATION REPORT NUMBER AFIT/GE/ENG/93D-09	
9. SPONSORING / MONITORING AGENCY NAME(S) AND ADDRESS(ES) Richard A. Kitzerow, WL/AARM-3, Wright-Patterson AFB OH 45433			10. SPONSORING / MONITORING AGENCY REPORT NUMBER	
11. SUPPLEMENTARY NOTES				
12a. DISTRIBUTION / AVAILABILITY STATEMENT Approved for public release; distribution unlimited			12b. DISTRIBUTION CODE	
13. ABSTRACT (Maximum 200 words) Fighter aircraft equipped with X-Band radars having an adaptive beamforming capability exhibit degraded performance due to radome multipath reflection (RMR). The reflections from the radome into the antenna array degrade the pattern and cause the formation of large sidelobes. This phenomenon makes detection of LO targets difficult when jamming enters the high RMR sidelobes. Actual radomes are curved and cause reflected wavefronts to be nonplanar. Analyzing beamformer performance under these conditions is difficult, since the beamformer response is defined as the amplitude and phase change experienced by a complex plane wave as a function of frequency and location. To work with planar wavefronts and for the sake of simplicity, we model the radome as two flat plates parallel to array broadside (one at each end of the array). This radome model demonstrates degraded beamformer performance by causing large sidelobes to form. This approximates the characteristics of the multipath environment caused by a real radome. The ability of a linearly constrained, minimum variance beamformer to cancel interference arriving in the sidelobes is evaluated. The cancellation performance depends on how many taps are employed and the source frequency bandwidth. Results are provided for a linear, equally spaced sixteen element array.				
14. SUBJECT TERMS Adaptive Beamforming, Radome Internal Reflection, Linearly Constrained Minimum Variance Beamforming, Adaptive Cancellation Performance			15. NUMBER OF PAGES 90	
			16. PRICE CODE	
17. SECURITY CLASSIFICATION OF REPORT UNCLASSIFIED	18. SECURITY CLASSIFICATION OF THIS PAGE UNCLASSIFIED	19. SECURITY CLASSIFICATION OF ABSTRACT UNCLASSIFIED	20. LIMITATION OF ABSTRACT UL	